Biochimica et Biophysica Acta 1838 (2014) 3036–3051

Contents lists available at ScienceDirect

Biochimica et Biophysica Acta

journal homepage: www.elsevier.com/locate/bbamem

One motif to bind them: A small-XXX-small motif affects transmembrane domain 1 oligomerization, function, localization, and cross-talk between two yeast GPCRs☆

Antonia Lock [a,1], Rachel Forfar [b,1], Cathryn Weston [b], Leo Bowsher [c], Graham J.G. Upton [d], Christopher A. Reynolds [d], Graham Ladds [b,*,2], Ann M. Dixon [c,**,2]

[a] Department of Genetics, Evolution and Environment, University College London, WC1E 6BT London, UK
[b] Division of Biomedical Cell Biology, Warwick Medical School, Coventry, CV4 7AL, UK.
[c] Department of Chemistry, University of Warwick, Coventry CV4 7AL, UK
[d] School of Biological Sciences, University of Essex, Wivenhoe Park, Colchester CO4 3SQ, UK

ARTICLE INFO

Article history:
Received 13 February 2014
Received in revised form 13 August 2014
Accepted 14 August 2014
Available online 23 August 2014

Keywords:
GPCR
TOXCAT
Oligomerization
Trafficking
Signaling
Cross-talk

ABSTRACT

G protein-coupled receptors (GPCRs) are the largest family of cell-surface receptors in mammals and facilitate a range of physiological responses triggered by a variety of ligands. GPCRs were thought to function as monomers, however it is now accepted that GPCR homo- and hetero-oligomers also exist and influence receptor properties. The *Schizosaccharomyces pombe* GPCR Mam2 is a pheromone-sensing receptor involved in mating and has previously been shown to form oligomers in vivo. The first transmembrane domain (TMD) of Mam2 contains a small-*XXX*-small motif, overrepresented in membrane proteins and well-known for promoting helix–helix interactions. An ortholog of Mam2 in *Saccharomyces cerevisiae*, Ste2, contains an analogous small-*XXX*-small motif which has been shown to contribute to receptor homo-oligomerization, localization and function. Here we have used experimental and computational techniques to characterize the role of the small-*XXX*-small motif in function and assembly of Mam2 for the first time. We find that disruption of the motif via mutagenesis leads to reduction of Mam2 TMD1 homo-oligomerization and pheromone-responsive cellular signaling of the full-length protein. It also impairs correct targeting to the plasma membrane. Mutation of the analogous motif in Ste2 yielded similar results, suggesting a conserved mechanism for assembly. Using co-expression of the two fungal receptors in conjunction with computational models, we demonstrate a functional change in G protein specificity and propose that this is brought about through hetero-dimeric interactions of Mam2 with Ste2 via the complementary small-*XXX*-small motifs. This highlights the potential of these motifs to affect a range of properties that can be investigated in other GPCRs.

G protein-coupled receptors (GPCRs) form a large ubiquitous family of transmembrane receptors that share a common topology of seven α-helical transmembrane domains (TMDs). GPCRs are conserved in all eukaryotes, where they act as key regulators of many cellular processes by triggering intracellular signaling cascades in response to environmental stimuli. Although alternative modes of activation exist, transmission of information across the lipid bilayer is commonly achieved by binding of ligand in the GPCR binding pocket, which forces a conformational change in the receptor's transmembrane domains [1,2]. This typically leads to G-protein binding, GDP–GTP exchange on the associated G protein, and propagation of the signal. GPCRs have also been shown to form dimeric or higher order oligomeric complexes, which may be a prerequisite for the correct subcellular targeting and functioning of the receptor [3,4] and may modulate receptor function [5]. Hetero-association of two (or more) GPCRs to form new receptor complexes that participate in "cross-talk" has also been reported, leading to

Abbreviations: GPCR, G protein-coupled receptor; TMD, transmembrane domain; CAT, chloramphenicol acetyltransferase; GpA, Glycophorin A; DMM, defined minimal media; GFP, green fluorescent protein; MBP, maltose binding protein; CHI, CNS searching of helix interactions; RMSD, room mean squared deviation; PVDF, polyvinyl difluoride; ECL, enhanced chemiluminescent substrate; S.E.M., standard error of the mean

☆ This work was funded by an EPSRC studentship through the MOAC Doctoral Training Centre (A.L.), an EPSRC pre-doctoral traineeship (A.L.), BBSRC CASE studentships with Septegen (R.F.), a Warwick Impact Fund (C.W. and G.L.), the University Hospitals of Coventry and Warwickshire NHS Trust (G.L.), the Biotechnology and Biological Sciences Research Council grant number (BB/G01227X/1) (G.L.) and Birmingham Science City Research Alliance (G.L.).

* Corresponding author. Tel.: +44 2476 150220; fax: +44 2476 523701.
** Corresponding author. Tel.: +44 2476 150037; fax: +44 2476 524112.
E-mail addresses: graham.ladds@warwick.ac.uk (G. Ladds), ann.dixon@warwick.ac.uk (A.M. Dixon).
[1] These authors contributed equally to the data shown in the manuscript.
[2] These authors contributed equally to the project.

http://dx.doi.org/10.1016/j.bbamem.2014.08.019
0005-2736/

modified G protein coupling and signaling [6]. Despite these and other excellent studies highlighting the importance of GPCR homo- and hetero-oligomerization, the specific interactions mediating complex formation are poorly understood due to the significant technical challenges involved in structural characterization of membrane proteins.

Lower eukaryotes are attractive model organisms in which to study GPCRs as they are amenable to genetic manipulation and exhibit less cross-talk between signaling pathways [7]. Several studies of the GPCR Ste2, the pheromone receptor from the budding yeast *Saccharomyces cerevisiae* which mediates the mating response, agree that oligomerization of this protein is facilitated (at least in part) by interactions involving transmembrane domain 1 (TMD 1) [8–11]. These interactions were further traced to a small-*XXX*-small motif (specifically a G_{56}-*XXX*-G_{60} motif) in TMD 1 [12]. Small-*XXX*-small motifs are motifs of two residues (typically glycine, but also alanine or serine) separated by three amino acids in the polypeptide chain, thus physically placing them on the same face of an α-helix. Co-location of these two small residues results in a "groove" which allows two helices to interlock via many favorable van der Waals contacts, thereby promoting helix–helix interactions. While these motifs have been frequently found at the oligomeric interface of helical membrane proteins [13–16], they have also been shown to be highly dependent upon the surrounding amino acid sequence [17,18], and are not always effective in driving protein interactions. Therefore, simple identification of these motifs in the primary sequence of a transmembrane domain is not a silver bullet to understanding protein interactions, but their presence can be used to design targeted mutagenesis strategies to verify their role (or lack thereof) experimentally. In this way, mutation of the G-*XXX*-G motif in Ste2 TMD 1 was shown in one study to interfere with oligomerization and localization (but not ligand binding) of the receptor [12]. However, other studies before and since have reported that Ste2 TMD 1 is not sufficient to drive oligomerization on its own, and that other domains in the receptor are also involved in complex formation including the N-terminus and TMD 2, TMD 4, and TMD 7 [9–11]. Evidence also exists that suggests the sites of contact between receptors change upon ligand-binding [9]. Moreover, it should be noted that, while small residues may mediate TMD packing, this is not always essential and indeed some GPCRs have been known to include more bulky residues such as isoleucine and leucine. In short, this growing body of work has not yet yielded a consensus model for Ste2 oligomerization, apart from the agreement that TMD 1 participates in some way.

The *Schizosaccharomyces pombe* P-factor receptor Mam2 [19] is orthologous to the Ste2 receptor, and immunoblotting (performed under non-denaturing conditions) has suggested the existence of oligomeric complexes [20] although a direct interaction has not been determined. Unfortunately, classical approaches to confirm dimerization of Mam2 have proven unsuccessful. In the past we have been able to immunoprecipitate heterologously expressed mammalian receptors from *S. pombe* cells [20,21], but somewhat surprisingly this has not been possible for Mam2 despite the production of two in-house antibodies. Likewise, we have been unable to utilize fluorescent-based techniques such as Förster resonance energy transfer (FRET) and bioluminescence resonance energy transfer (BRET) due to the large size of the C-terminal tail of Mam2 (45 amino acids). Unlike Ste2, where it has been possible to delete the C-terminal tail and still produce a functional receptor [12], Mam2 has an absolute requirement of its C-terminal tail to facilitate efficient downstream signal transduction [22]. The tail of Mam2 is absolutely required for an interaction with the regulator of G protein signaling 1 (Rgs1) protein that both negatively and positively modulates signal transduction dependent upon the dose of stimulating pheromone [22,23]. Deletion of the Mam2 C-terminal tail generates a receptor with severely attenuated signaling abilities. Consequently, a novel approach that attempts to understand the Mam2 dimerisation interface has been required and we described here our use of the bacterial expression system TOXCAT [24] to investigate the Mam2 dimerization interface.

Along with the suggestion that Mam2 forms oligomers [20], Mam2 further resembles Ste2 in that it also contains two consecutive small-*XXX*-small motifs (G_{49}-*XXX*-S_{53}, S_{53}-*XXX*-A_{57}) in TMD 1. Given the lack of a consensus as to the precise mechanisms governing oligomerization of fungal GPCRs, and guided by previous studies of Ste2 as well as the presence of well-known helix interaction motifs, we describe here for the first time the effects of targeted mutation of the small-*XXX*-small motifs on oligomerization, function, and localization of Mam2. Equivalent experiments were performed on Ste2 for comparison to Mam2 and the wider literature. Our results demonstrate that the TMD 1 small-*XXX*-small motifs play a critical part in the correct localization and function of full-length Mam2, and this behavior is mirrored in parallel experiments performed on Ste2. The small-*XXX*-small motifs also promote strong self-association of Mam2 TMD 1 in isolation (a result which is not observed in parallel experiments on Ste2 TMD 1). Using a series of chimeric G protein expressing strains [21], we also demonstrate that Mam2 can form functional heterodimers with Ste2, and our mutagenesis data suggest that this occurs via complementary small-*XXX*-small motifs in the first TMD of each receptor. Molecular models of the relevant helix–helix interactions are used to support the experimental results and illustrate plausible interaction modes. The data presented here highlight the importance of this well-known motif and offer novel insight into the mechanisms used by Mam2 to functionally assemble into homo- and hetero-oligomeric complexes.

1. Materials and methods

1.1. TOXCAT assay and construction of chimera

The self-association of the first transmembrane domains of *S. cerevisiae* Ste2 (V_{49}–W_{70}) and *S. pombe* Mam2 (L_{46}–C_{67}) were studied using the TOXCAT assay, which has been described previously [24]. Briefly, the DNA sequence encoding the transmembrane domain of interest was cloned into the pccKAN vector between the dimerization-dependent DNA binding domain of ToxR at the N-terminus, and maltose binding protein (MBP) at the C-terminus. The resulting fusion protein was expressed in *Escherichia coli* NT326 cells lacking endogenous MBP. TM domain-driven oligomerization of the fusion protein leads to ToxR mediated activation of the reporter gene chloramphenicol acetyltransferase (CAT), with CAT expression levels indicating the strength of TM self-association. Before performing assays, correct insertion and orientation of the TOXCAT constructs in the *E. coli* inner membrane was confirmed using the protease sensitivity in spheroplast assay [24]. Expression levels for all constructs were determined via western blots against maltose binding protein (MBP). The chloramphenicol acetyltransferase (CAT) reporter gene was quantified using the FAST CAT kit (Invitrogen). CAT activity was normalized to the expression level of each construct using the ImageJ tool [25] to quantify band intensities on a western blot, and all CAT activities are reported relative to the value obtained for the positive control, the strongly-dimerizing TMD of Glycophorin A (GpA). A point mutant of GpA, G_{83}I, which impairs TMD association, was used as a negative control. Values given are the means (±S.D.) for three or more independent measurements and a student's T-test was performed to determine the significance of changes in CAT activity.

1.2. Yeast strains, plasmid construction and culture conditions

The yeast strains used in this study are listed in Table S1. All yeast strains were derived from JY546 which contains the *sxa2* > *lacZ* construct for quantification of pheromone-dependent transcription. To facilitate the expression of heterologous GPCRs in *S. pombe*, we have previously described the generation of a series of Gα-transplants, integrated at the *gpa1* locus, in which the C-terminal five amino acids of Gpa1 were replaced with the corresponding residues from mammalian Gα-subunits [21]. General yeast procedures are as described previously

[26,27] using lithium acetate for the transformation of yeast. Culture media used was DMM (a defined minimal media for selective growth and all assays). The pREP vectors allow expression of genes under the control of the thiamine-repressible, *nmt1* promoter; pREP3x contains the nutritional selection marker *LEU2* and pREP4x, and *ura4* [28]. *S. pombe* genes were amplified from genomic DNA via PCR using FastStart high fidelity polymerase blend (Roche Diagnostics Ltd., UK) and cloned into the pREP vectors. All Ste2 and Mam2 mutations were generated by inverse PCR and constructs sequenced to ensure faithful amplification. Fluorescent and Gpa1 fusion constructs were generated using a two-step cloning technique as described previously [21]. The Ste2 open reading frame was amplified using JO1372 (ATGTCTGATG CGGCTCCTTC; upper case letters are complementary to positions 1 to 20) and JO1373 (TAAATTATTATTATCTTCAG; upper case letters are complementary to positions 1293 to 1274) removing the stop anti-codon from the ORF, and were cloned into unique *Eco*RV sites of JD1698 (a modified version of the pREP vector containing the GFP ORF with an *Eco*RV site immediately upstream of the initiator codon of GFP), JD1773 (pREP containing Gpa1) and JD2735 (pREP the inactive mutant of Gpa1 [G242A]) [20]. We have previously described the generation of Mam2-Gpa1 and Mam2-Gpa1 [G242A] constructs [20].

1.3. Assay of β-galactosidase activity

Assays were performed as described previously [21,29]. Cell concentrations were determined using a Coulter Channelyser (Beckman Coulter).

1.4. Computational searches using CHI

Structural calculations were performed using the CNS searching of helix interactions (CHI) software package, which has been previously described [30,31], on an 8-node dual 2.66-GHz Xenon processor Linux cluster (Streamline Computing, Warwick). CHI was used to create homodimer models from two parallel α-helices containing the predicted sequences of either Mam2 or Ste2 TMD 1 (L_{46}–L_{61} and V_{49}–I_{67} for Mam2 and Ste2, respectively), using previously published parameters for the search (e.g. starting crossing angle and interhelical distance, and rotation step size) [14]. Heterodimer models were created from parallel α-helices containing residues V_{49}–W_{70} of Ste2 and L_{46}–C_{67} of Mam2 using the same starting parameters described above. Groups of a minimum of 10 structures with a backbone RMSD of ≤1 Å were clustered and the average structure for each cluster was calculated. In the case of homo-dimers, only clusters containing symmetrical dimers were considered. Each search was carried out three to five times to check for frequency of a given model.

1.5. Model GPCR dimeric structures

A number of GPCR crystal structures contain dimers within the asymmetric unit, and while some are clearly not biologically meaningful, others present TMD 1 as part of the dimeric interface. The PISA software [32], www.ebi.ac.uk, is useful for addressing whether a crystallographic dimer is the correct biological dimer and can also identify other dimeric interfaces within the crystal lattice. In order to analyze whether any of these GPCR dimeric structures [33] are relevant, we have aligned TMD 1 of 112 Ste2/Mam2 homologues to class A/class B/class C/class E GPCR homologues. The position of TMD 1 for the Mam2 receptor was predicted using the topology prediction tool TMHMM [34]. These alignments are within or below the twilight zone, and so are potentially difficult, but elsewhere we have presented a novel alignment method that correctly aligned the known TMDs for class A and B GPCRs [35]. The method is essentially based on a helix by helix profile alignment, with the following additional features. Firstly, all pairwise alignments are considered and each possible alignment receives a vote if it is the top scoring pairwise alignment. Secondly, entropy is included via a maximum lagged correlation [36]. Elsewhere we also included amino acid volume [35] and hydrophobicity [35,36], but here we restrict ourselves to the more reliable pairwise alignments and entropy. The approaches are combined by scaling the votes (or the correlation coefficients) between 0 and 1 and multiplying together, so that alignments that receive minimum support are eliminated and alignments that receive strong support are promoted. Here we additionally included the product of pair wise alignments over multiple classes, and similarly for entropy. The alignment enabled us to map the G-*XXX*-G motifs onto the opsin dimer (PDB code 3CAP) [37].

1.6. Confocal microscopy

Measurements were performed as described previously [22,38]. Strains cultured in DMM were harvested washed twice in fresh growth medium and transferred to poly-lysine-coated slides (Sigma-Aldrich Co. Ltd.). Cells were viewed using a Personal DeltaVision (Applied Precision, Issaquah, WA) comprising, an Olympus UPlanSApo 100×, N.A. 1.4, oil immersion objective and a Photometric CoolSNAP HQ camera (Roper Scientific). Captured images were processed by iterative constrained deconvolution using SoftWoRx (Applied Precession) and analyzed using ImageJ. All images were captured in a z-stack with the highest intensity chosen.

1.7. Image analysis

Image analysis was performed using the open source program ImageJ (http://rsb.info.nih.gov/ij/). Cell segmentation was achieved using the BOA plug-in component of the Quantitative Imaging of Membrane Proteins (Quimp) package (http://go.warwick.ac.uk/bretschneider/quimp) [39–41]. 30 yeast cells were selected at random for analysis as previously described [39] and representative images were shown. For many of the GPCRs analyzed in this study, cell surface expression was significantly impaired. This reduction in cell surface expression correlated with a reduction in the magnitude of the signaling. To provide a quantitative comparison of all receptors measured, we corrected the extent of signaling by accounting for the percentage of cell surface expression. The wildtype receptors were used as our reference. We have used similar techniques previously to correct signaling responses where ligands have had toxic affects [38].

1.8. Immunoblotting of GPCRs

Plasma membrane extracts were prepared from yeast strains containing various pREP vectors expressing the different Mam2 and Ste2 constructs grown in minimal medium lacking thiamine to ~1×10 [7] cells ml^{-1} using the method described [20]. Samples were resolved using non-denaturing SDS-PAGE and transferred to polyvinyl difluoride (PVDF) membrane with a semidry blotter. Western blotting was performed using a rabbit GFP monoclonal antibody (Santa Cruz Biotechnology Inc, Santa Cruz, California, USA) or a rabbit polyclonal anti-6-His (Abcam, Cambridge, UK) as the primary antibody as appropriate. A donkey anti-rabbit IgG horse-radish peroxidase (HRP) conjugate (Amersham, International, Little Chalfont, Buckinghamshire, UK) was used as the secondary antibody. Antibodies were used according to the manufacturers' instructions. HRP activity was detected using ECL substrate (Amersham).

1.9. Data analysis

Data were analyzed using GraphPad Prism v6.0c for Mac OS X (GraphPad Software Inc, San Diego, CA). Concentration response curves were fitted using the three-parameter logistic equation to obtain pEC_{50} for agonists. The operational model for partial agonism [42] was used to

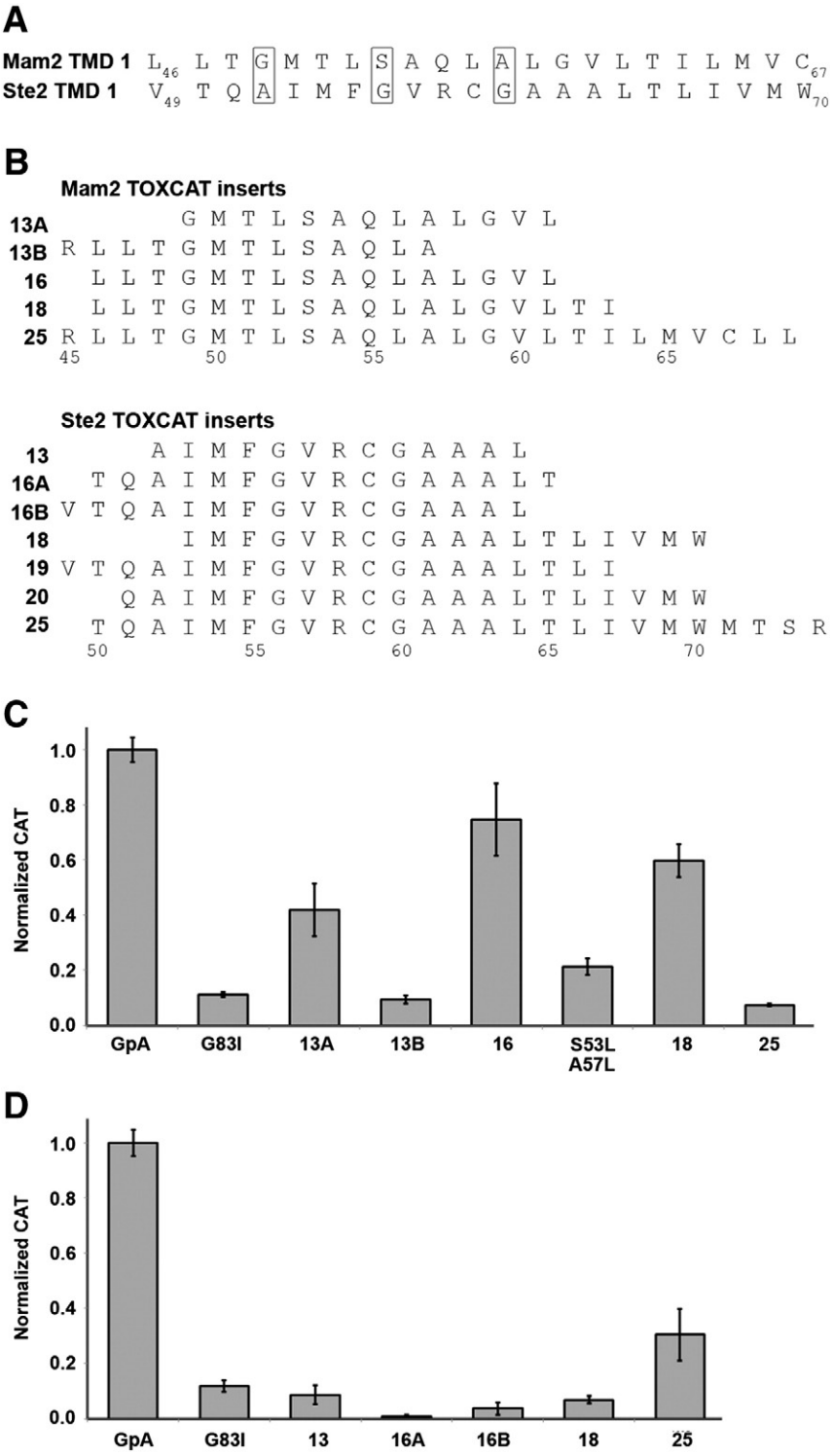

Fig. 1. Mam2 TMD 1, but not Ste2 TMD 1, self-associates strongly in a biological membrane via the S_{53}-XXX-A_{57} motif. (A) Alignment of the primary sequences of putative transmembrane domain 1 (TMD 1) in the *S. pombe* Mam2 and *S. cerevisiae* Ste2 receptor. The small-XXX-small motifs are boxed. (B) Sequences of the Mam2 and Ste2 TMD 1 TOXCAT inserts that were studied in this report. The TOXCAT system (as detailed in Materials and methods) is sensitive to the length and sequence of the TMD insert, so multiple sequence inserts were tested. (C) CAT activities obtained in the TOXCAT assay for the wild-type and mutant Mam2 TMD 1 constructs. (D) CAT activities obtained in the TOXCAT assay for the wild-type Ste2 TMD 1 constructs. CAT activities were normalized to expression level of each construct and the CAT activity of the positive control, GpA. Results are means ± S.E.M. for triplicate measurements from three independent isolates.

obtain relative values of efficacy ($\log \tau$) and the equilibrium dissociation constant ($\log K_A$). Results are expressed as means ± S.E.M. unless otherwise stated. Statistical analyses were performed by using a one-way ANOVA with a Tukey's multiple comparison post-test, or one-way analysis of variance followed by Bonferroni's post-test, as appropriate. Values of $p < 0.05$ were considered statistically significant.

2. Results

2.1. Conservation of small-XXX-small motifs in TMD 1 of Mam2 and Ste2 and other class A/B/C/E GPCR sequences

Inspection of the primary sequence of TMD 1 from the Mam2 receptor, predicted using the topology prediction tool TMHMM [34] revealed

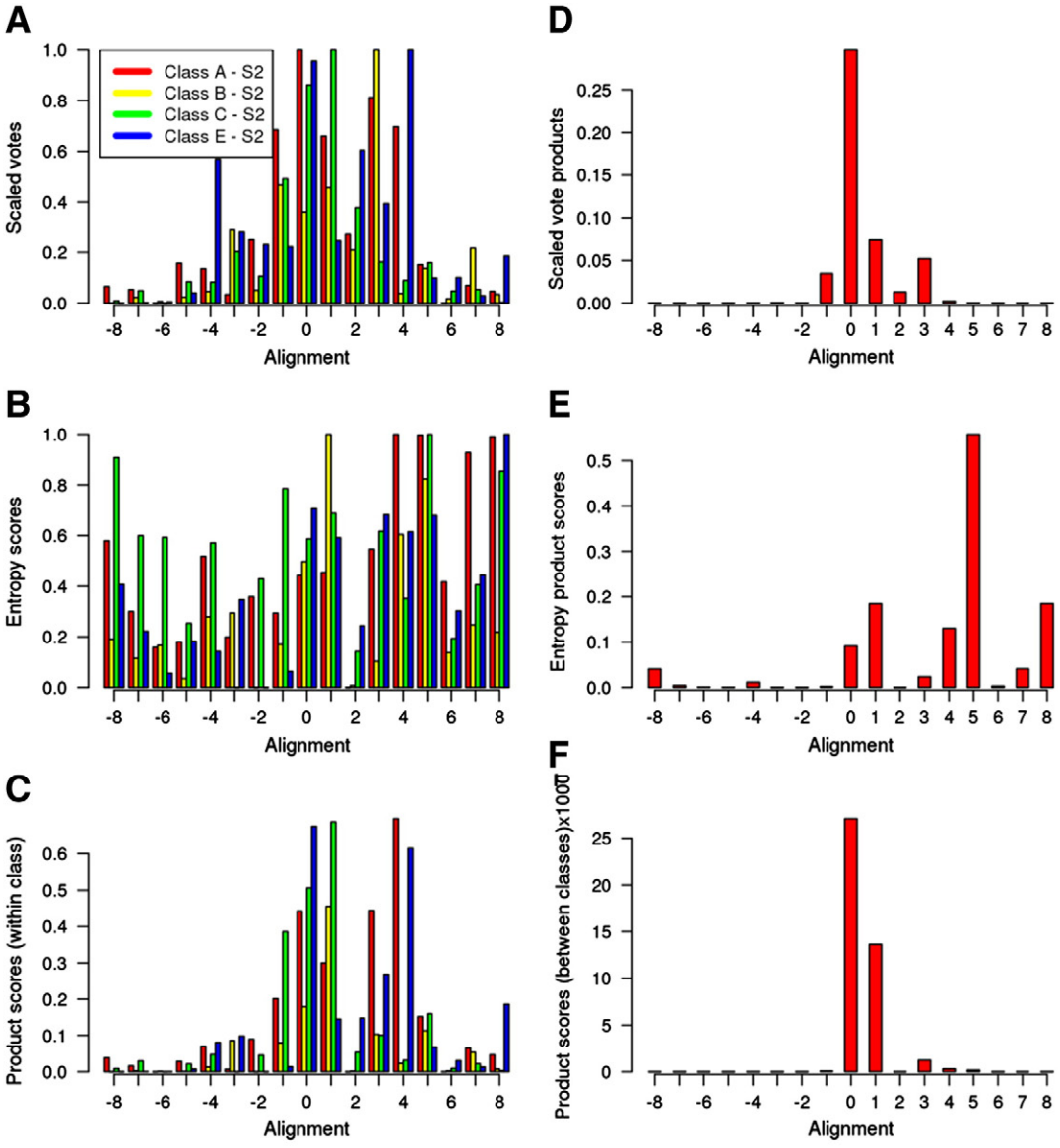
A
Class A - S2
Class B - S2
Class C - S2
Class E - S2
Scaled votes
Alignment
D
Scaled vote products
Alignment
B
Entropy scores
Alignment
E
Entropy product scores
Alignment
C
Product scores (within class)
Alignment
F
Product scores (between classes)x1000
Alignment

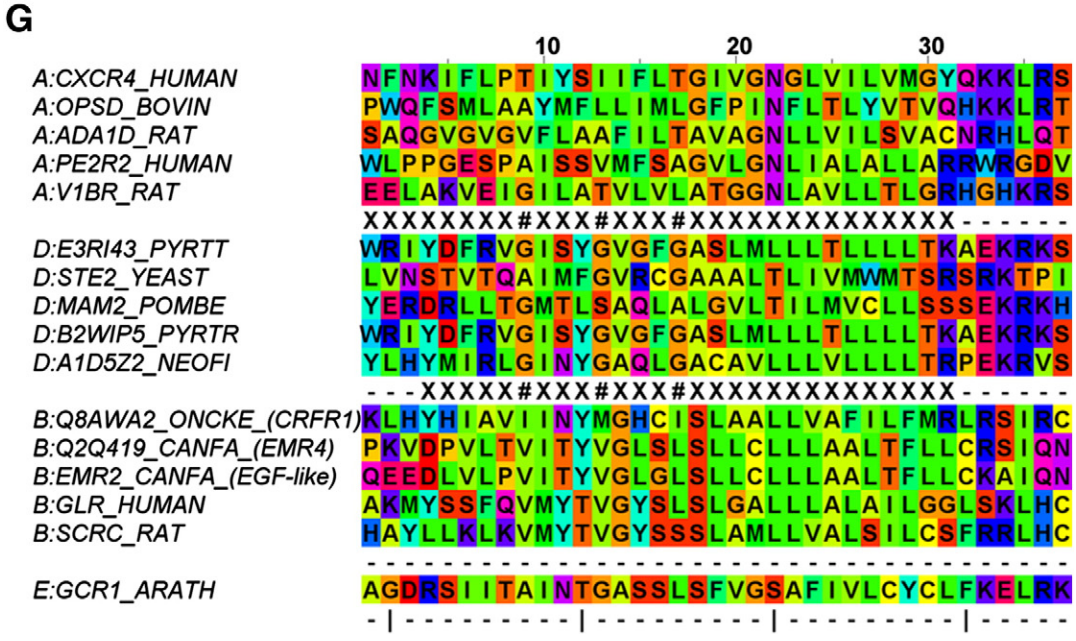
G
10
20
30
A:CXCR4_HUMAN
A:OPSD_BOVIN
A:ADA1D_RAT
A:PE2R2_HUMAN
A:V1BR_RAT
D:E3RI43_PYRTT
D:STE2_YEAST
D:MAM2_POMBE
D:B2WIP5_PYRTR
D:A1D5Z2_NEOFI
B:Q8AWA2_ONCKE_(CRFR1)
B:Q2Q419_CANFA_(EMR4)
B:EMR2_CANFA_(EGF-like)
B:GLR_HUMAN
B:SCRC_RAT
E:GCR1_ARATH

that it contains two consecutive small-*XXX*-small motifs; G_{49}-*XXX*-S_{53} and S_{53}-*XXX*-A_{57} (boxed, Fig. 1A). The same is true for the Ste2 receptor TMD 1, containing both A_{52}-*XXX*-G_{56} and G_{56}-*XXX*-G_{60} motifs (although only the G_{56}-*XXX*-G_{60} motif has been highlighted in the literature). Sequence alignment of the full-length Mam2 and Ste2 proteins using Clustal [43,44] revealed that the Ste2 G_{56}-*XXX*-G_{60} motif in TMD 1, shown previously to affect oligomer formation and function of the receptor [12], aligns to the more C-terminal small-*XXX*-small motif in Mam2 TMD 1 (S_{53}-*XXX*-A_{57}, see Fig. 1A). The alignment was produced using the full-length proteins, but only the sequences of the first TMD are shown for clarity. The alignment of the full-length proteins revealed a low sequence identity between the two (see Fig. S1 for full-length alignment), reflecting their long evolutionary distance.

We have previously described a new approach to enable the alignment of GPCR family TMs [35,36]. We observed that GCR1, the only well-characterized plant GPCR, had sequence similarity to both class A and class B GPCRs and that class E homologues have been proposed as the ancestral sequences for class A and class B GPCRs. Using this evidence we were able to align class A GPCRs with class B. Thus, to provide a comprehensive analysis of the conservation of the small-*XXX*-small motif in other Class D GPCRs as well as other families of GPCRs, we aligned Mam2/Ste2 homologues (class D) to class A, class B, class C and class E GPCRs (the class A/B/C/E alignment is well defined [35,45] so an alignment to class A defines the alignment to class B etc.). We generated consensus scores from two different analyses (helical alignment and entropy correlation coefficients). Fig. 2A shows the pairwise helical alignments evaluated, using the PHAT matrix, of 17 alternative variants for Mam2/Ste2 homologue TM1 to class A, class B, class C and class E. All alternatives yield different preferred alignments, however, when scaled (Fig. 2D) we see a distinct preference for alignment 0, which we report for the predicted TM1 and flanking regions of several GPCRs in Fig. 2G. We next evaluated the alignments using entropy (Fig. 2B/E). While entropy does not necessarily favor the correct alignment, it usually gives a reasonable score for the correct alignment [35]. Fig. 2C shows the product of the scaled votes for the pairwise alignments multiplied by the scaled entropy scores for the alignments over all four classes and again we see a strong preference for alignment 0 (Fig. 2F). Given that the pairwise scores are more reliable than the entropy scores, the results in Fig. 2D should be given the strongest weight. Thus, the Class A/Mam2/Ste2/Class B and Class E alignment 0 is given in Fig. 2G (from which the alignment to Class C can be inferred [35,45]). From inspection of the primary sequences in this alignment we can see that the small-*XXX*-small motifs in Ste2 and Mam2 are conserved across several members of Class D GPCRs, but these motifs are only weakly conserved in other classes.

2.2. Strong, sequence-dependent oligomerization of Mam2 (not Ste2) TMD 1

The propensity for TMD 1 in Mam2 (and Ste2 for comparison) to self-associate in isolation was assessed using the TOXCAT assay. This assay allows inducible (if required) expression of a TM domain of interest as part of a fusion protein, and qualitative evaluation of the propensity of that TM helix to self-associate in a natural (albeit not always native) bacterial membrane. It offers a relatively straightforward and robust platform upon which to screen the effects of point mutations, and has provided a means to investigate sequence specific interactions for membrane proteins that are extremely difficult to express and purify in their full-length forms. One of the main drawbacks of this assay is that it is most appropriate for the study of single transmembrane domains, which can complicate data interpretation when studying multi-spanning membrane proteins. An additional trait of this assay is that, in our hands [14] and in other labs [46] this system is sensitive to the length and amino acid sequence of the TMD inserted, therefore five different constructs containing Mam2 TMD 1 sequences of varying lengths and sequence frames were prepared (Fig. 1B). To compare the Mam2 results in this assay to similar results for Ste2 TMD1 (which has never been investigated using the TOXCAT assay), we prepared seven different constructs containing Ste2 TMD 1 inserts (Fig. 1B). Alongside these constructs, we also measured the oligomerization of the strongly dimerizing Glycophorin A TMD (positive control) and the G_{83}I mutant of this domain which destabilizes the dimer (negative control) as described previously [24].

The CAT activities for the various Mam2 TMD 1 constructs are shown in Fig. 1C. Western blots against MBP to demonstrate relative expression levels of the full-length chimeras (CAT activities were normalized to expression level) are shown in Figure S2 (panel A, see band at ~62 kDa). Mam2 TMD 1 was found to form intermediate-strong oligomers in the *E. coli* inner membrane (Fig. 1C, see constructs 13A, 16, and 18), yielding CAT activities of up to 75% that observed for GpA (construct 16). The position of the small-*XXX*-small motif in the membrane is known to influence the strength of helix–helix interactions, with motifs located near the center of the TMD capable of forming stronger interactions than motifs located near the lipid head group region [47]. The TOXCAT assay is also sensitive to the topology of the inserts, with insert length and the rotational positioning of the ToxR domains relative to each other influencing the expression of CAT [14,46,48]. We exploited the fact that centrally located motifs produce stronger TOXCAT signals to differentiate the roles of the two small-*XXX*-small motifs present in Mam2 TMD 1. Each motif was centered in the middle of a 13-amino acid insert, producing two constructs with slightly different sequences. Centering the S_{53}-*XXX*-A_{57} motif (13A in Fig. 1B) leads to a higher normalized CAT activity (42% of GpA) than centering the G_{49}-*XXX*-S_{53} motif (13B in Fig. 1B), which produced a normalized CAT activity 10% that of GpA (and equivalent to the negative control, G_{83}I).

Because the S_{53}-*XXX*-A_{57} motif appeared to be a stronger mediator of Mam2 TMD 1 dimer formation, S_{53} and A_{57} were mutated to Leu in the TOXCAT construct that yielded the highest degree of oligomerization (16 amino acid insert), and the CAT activity was re-measured. Leucine substitutions at these positions reduced the normalized CAT activity by 72% compared to wild-type TMD 1 (Fig. 1C), suggesting a substantial reduction in the strength of oligomerization when close packing of the S_{53}-*XXX*-A_{57} motif was disrupted.

For Ste2, western blots against MBP (Fig. S2, panel B) revealed that the constructs containing 19 and 20 amino acid TMD inserts were rapidly cleaved in vivo, leaving only MBP (see band at ~40 kDa) visible on the gels and suggesting the absence of full-length chimera. Therefore these two constructs were not investigated further. A significant amount of cleavage (>50%) was also observed for the 13 and 18 amino acid TMD constructs, and very low CAT activities were observed for both of these. Surprisingly, even for the remaining constructs

Fig. 2. The TMD1 sequence alignment between selected Mam2/Ste2 homologues and selected class A, selected class B sequences and GCR1. (A) The number of votes (scaled between 0 and 1) for each of the 17 alternative pairwise alignments evaluated using the PHAT matrix, denoted V_A, V_B, V_C and V_D respectively [75]. Alignment 0 corresponds to the alignment given in Figure 2G; alignment −1 corresponds to moving the S2 sequence 1 position to the left. The legend for panels A–C is shown in the box. (B) The maximum correlation values for each alignment evaluated using entropy (scaled between 0 and 1), denoted S_A, S_B, S_C and S_D respectively. (C) The preferred alignment as indicated by the product of the number of votes × entropy, i.e. $V_A \times S_A$, $V_B \times S_B$, $V_C \times S_C$ and $V_D \times S_D$. (D) The preferred alignment as indicated by the product of the scaled votes: $V_A \times V_B \times V_C \times V_D$. (E) The preferred alignment as indicated by the product of the scaled entropy: $S_A \times S_B \times S_C \times S_D$. (F) The preferred alignment as indicated by the product of the votes × entropy: $V_A \times V_B \times V_C \times V_D \times S_A \times S_B \times S_C \times S_D$. (G) Generic position 1.50 (the most conserved position in class A) is marked by a vertical bar and is the conserved N, at position 22. The helical region of rhodopsin and the corticotrophin releasing hormone receptor are marked by an 'X'. The Mam2/Ste2 small residues of the small-XXX-small-XXX-small motif are marked by '#'. These are not conserved as small residues in other classes. The color reflects the biophysical properties. The residues are color coded according to their properties as follows: blue, positive; red, negative or small polar; purple, polar; cyan, polar aromatic; green, large hydrophobic; yellow, small hydrophobic. This corresponds to the Taylor scheme, as implemented in Jalview [76].

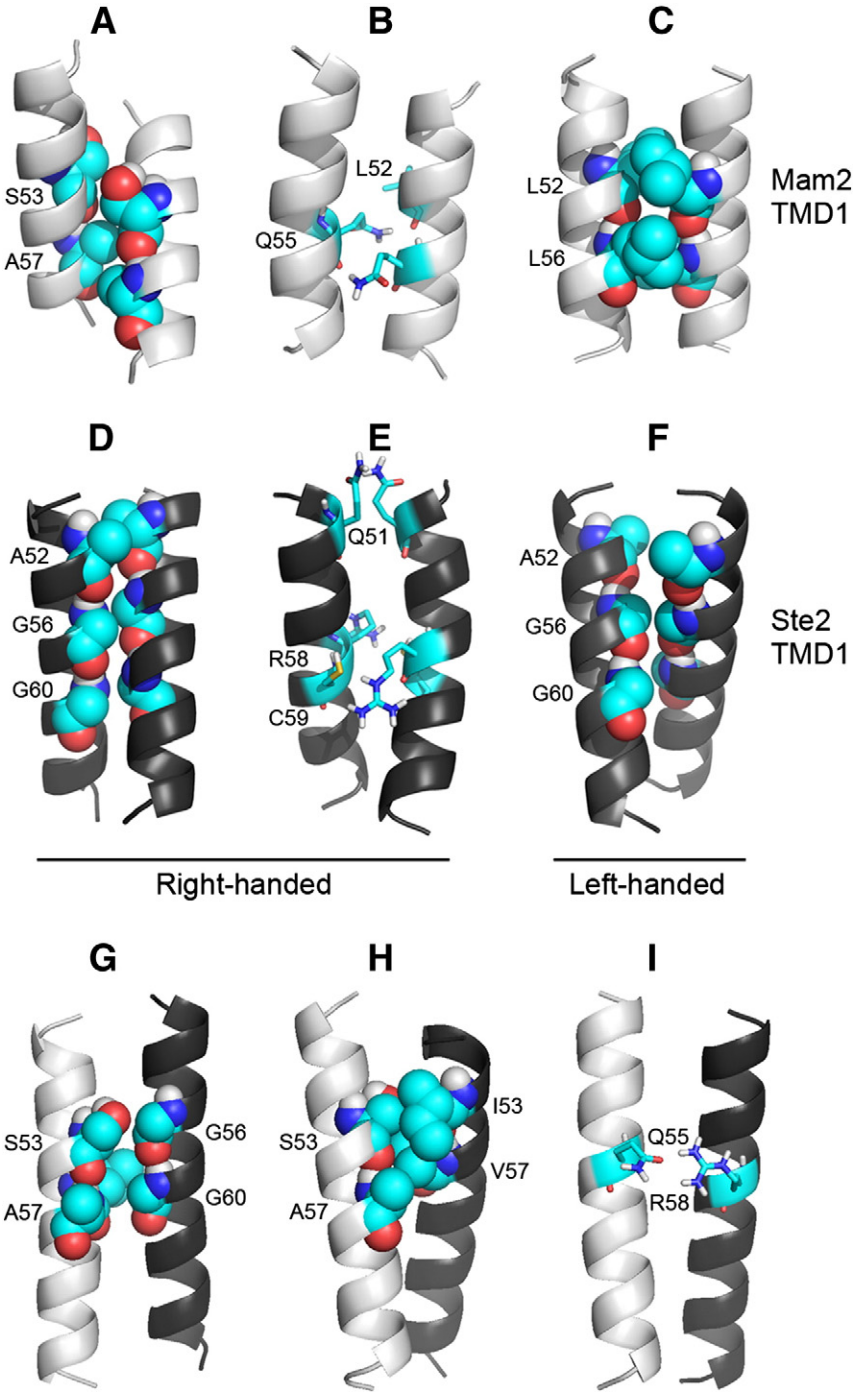

Fig. 3. Molecular models of the Mam2 and Ste2 TMD 1 homo- and hetero-dimers. The most frequently observed structures of the Mam2 homodimer in replicate searches contained the S_{53}-XXX-A_{57} motif at the dimer interface (A), however structures were also observed containing Q_{55} (B) and L_{52}-XXX-L_{56} at the dimer interface (C). Similar models were obtained for Ste2 TMD 1 homodimers, containing either A_{52}, G_{56}, and G_{60} (D and F) or polar residues (e.g. Q_{51} and R_{58}) at the dimer interface (E). Models obtained from multiple Mam2 (white) — Ste2 (black) hetero-dimer searches suggest that interactions are mediated either by the central small-XXX-small motif in both (G) or only one (H) helix, or a pair of polar residues (I). All models were obtained by performing searches using the program CHI (see Materials and methods).

investigated in the assay in which little to no cleavage occurred, Ste2 TMD 1 was not found to strongly oligomerize (Fig. 1D). The 25 amino acid TMD insert showed the highest CAT activity, which was only 30% that of GpA.

2.3. Homo-dimer models of Mam2 suggest packing of small-XXX-small motifs

The TOXCAT data suggest that, outside the context of the full-length GPCR, Mam2 TMD 1 strongly self-associates in a sequence dependent manner, while Ste2 TMD 1 only weakly self-associates. To better understand what structural features stabilize the oligomeric form of the TMD, computational models were produced using the program CHI [30,31]. The predominant Mam2 TMD 1 homo-dimer model observed across multiple searches was a symmetric, right-handed homo-dimer containing the S_{53}-*XXX*-A_{57} motif at the dimer interface (see Fig. 3A for a representative structure). We also observed a dimer mediated by an interhelical hydrogen bond between the side-chain amide of Q_{55} to the backbone carbonyl oxygen of L_{52} on the opposite helix (Fig. 3B, hydrogen bonds were assigned when a hydrogen bond donor and acceptor

were within 2.8 Å of one another). This solution was, however, not observed in every search, as was the S_{53}-*XXX*-A_{57} dimer. The only symmetrical left-handed dimer observed in multiple trials contained a motif of L_{52}-*XXX*-L_{56} (Fig. 3C), but this solution also did not occur in every search.

Homo-dimer searches for Ste2 TMD 1 were also carried out for comparison, despite the fact that this TMD showed very little propensity to self-associate in TOXCAT. As with Mam2, two general types of right-handed homodimers were observed for Ste2 TMD 1, one containing small-*XXX*-small motifs at the dimer interface (in this case A_{52}-*XXX*-G_{56}-*XXX*-G_{60}, Fig. 3D) and one in which a Gln residue (Q_{51}) forms intermolecular hydrogen bonds (Fig. 3E). The only symmetrical left-handed dimer observed also contained the A_{52}-*XXX*-G_{56}-*XXX*-G_{60} motif (Fig. 3F) at the dimer interface. Interestingly, we observed that the structures of Ste2 homo-dimers were all loosely-packed, with little to no close packing of the Gly residues.

2.4. Effects of mutations in the small-XXX-small motif on Mam2 function in vivo

Given the previously-demonstrated importance of the Ste2 G_{56}-*XXX*-G_{60} motif in oligomerization, signaling and trafficking [8,10,12] and the identification of a similar small-*XXX*-small motif that promotes TMD 1 interactions in Mam2, it remained to be investigated whether the S_{53}-*XXX*-A_{57} motif could have an impact on full-length Mam2 function in vivo. Cells expressing Mam2 were treated with increasing concentrations of pheromone (0–100 μM), and the ability of Mam2 to sense pheromone and relay the signal intracellularly was quantified by means of the reporter protein β-galactosidase, as described in the Materials and methods section. The ability of cells to respond to pheromone when expressing *Mam2* from the inducible *nmt1* promoter was comparable to expression of the gene from its

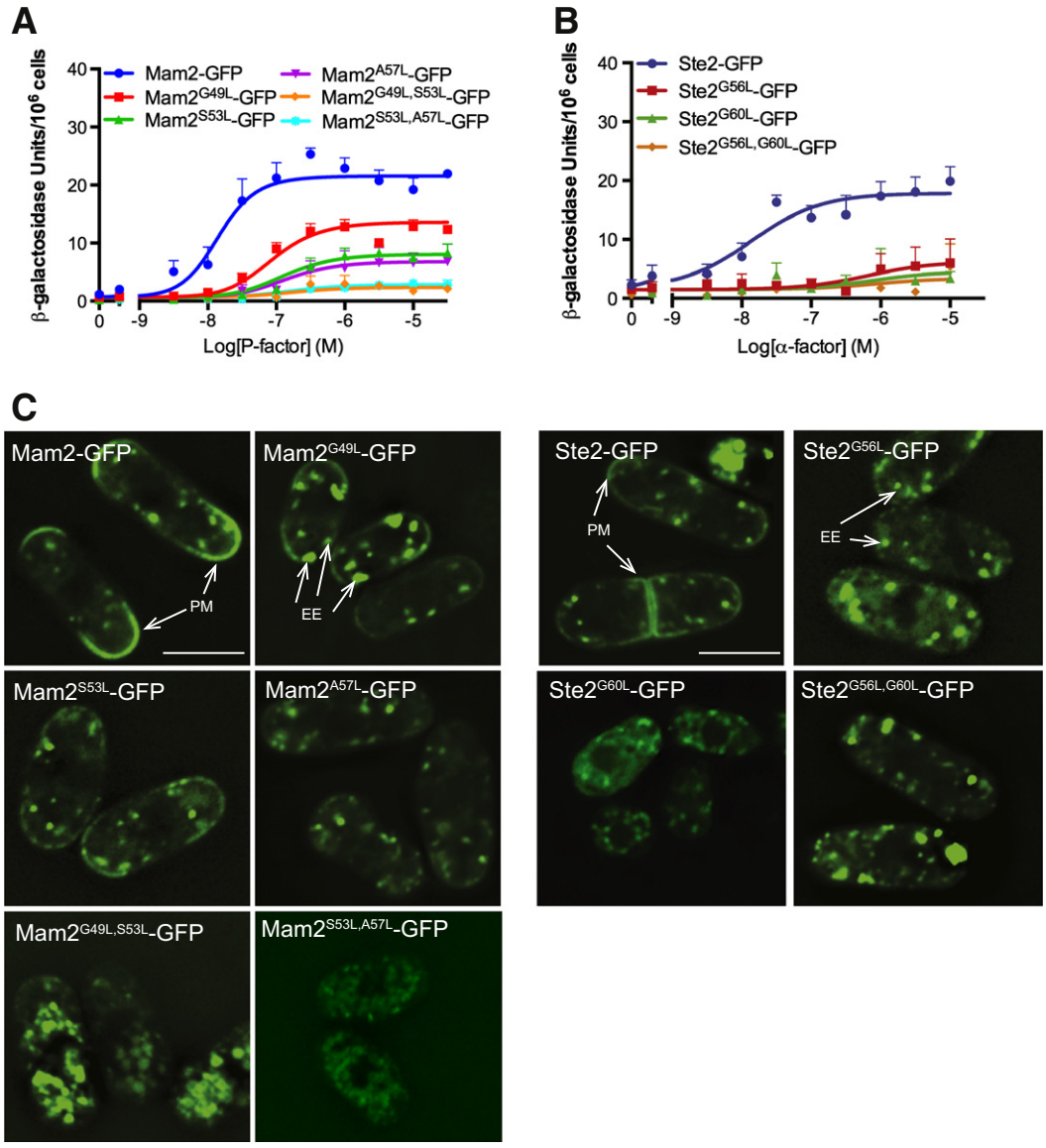

Fig. 4. Mutating the small-XXX-small motif reduces sensitivity to pheromone, maximal signaling and receptor localization. Pheromone dependent transcription of β-galactosidase expressed from the JY1169 Mam2-D10, sxa2 > lacZ reporter strain [21] was measured in yeast expressing GFP-tagged receptors from the inducible *nmt1* promoter; (A) wild-type Mam2 (●), $Mam2^{G49L}$ (□), $Mam2^{S53L}$ (▲), $Mam2^{A57L}$ (▼), $Mam2^{G49L,S53L}$ (♦), and $Mam2^{S53L,A57L}$ (×). (B) Wild-type Ste2 (●), $Ste2^{G56L}$ (□), $Ste2^{G60L}$ (▲), and $Ste2^{56L,G60L}$ (♦). Data was fitted using the operational model for receptor depletion. Results are means ± S.E.M. of triplicate determinations from three independent isolates. (C) Subcellular localization of the mutants was described in A and B. Plasma membrane (PM) and early endosome structures (EE) are highlighted. Scale bar 5 μm. (D) Percentage membrane fluorescence of the Mam2 mutants imaged in C. (E) Percentage membrane fluorescence of the Ste2 mutants imaged in C. Values shown are means ± SEM of 30 independent representative cells. Statistical significance from wildtype receptor (Mam2-GFP or Ste2-GFP) was determined using a one-way ANOVA with a Tukey's multiple comparison post-test; **representing $p < 0.01$ and ***representing $p < 0.001$. (F) Scaled responses for the Mam2 mutants shown in A but accounting for the differences in extend of plasma membrane localization from D. (G) Scaled responses for the Ste2 mutants shown in B and extend of plasma membrane localization from E.

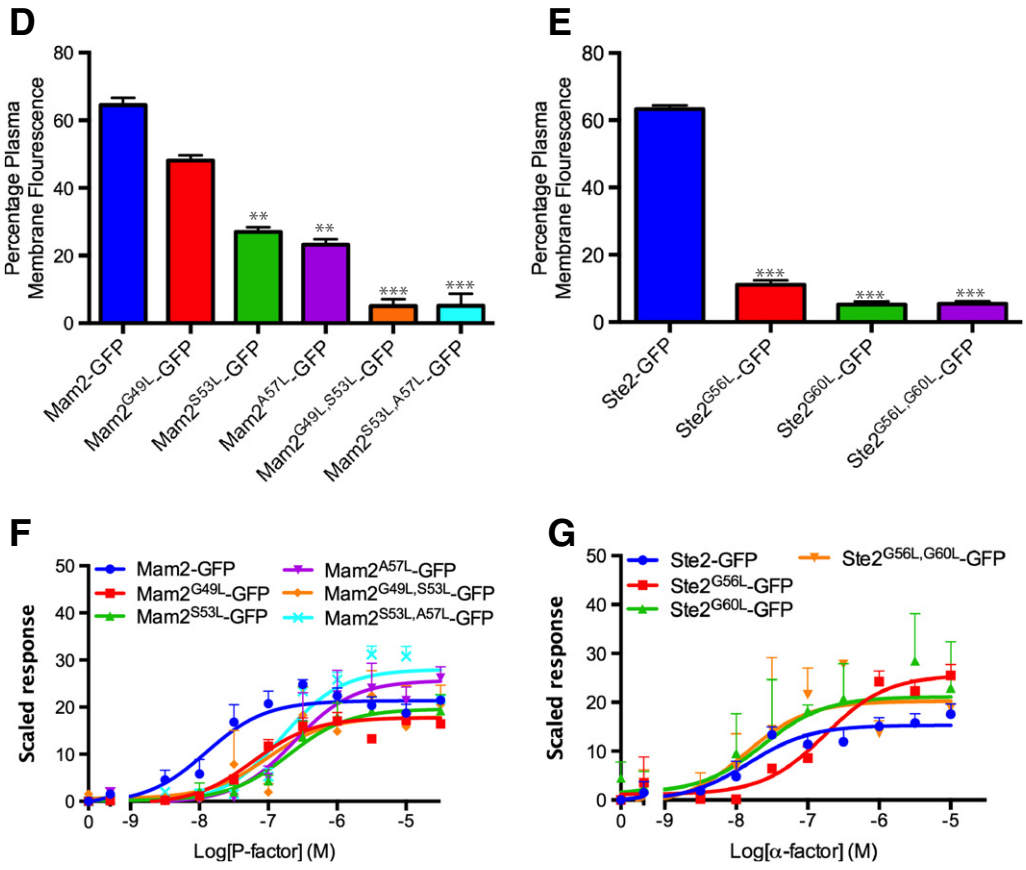

Fig. 4 (*continued*).

chromosomal locus [20]. We found that single point mutations of any of the small residues in the small-XXX-small motifs of Mam2 TMD 1 (G_{49}, S_{53} or A_{57}) to Leu resulted in the reduction of Mam2-derived cellular signaling (Fig. 4A). It appeared as though cells were affected both in their ability to sense pheromone, and in terms of maximal response elicited. The most pronounced effect was observed with the S_{53}L and A_{57}L mutations, although the G_{49}L mutation also had an effect. This is not unexpected as G_{49} is predicted to lie on the same helical face as S_{53} and A_{57}, although residues located close to the TM core tend to contribute more strongly to helix–helix interactions [47]. We also found that simultaneous mutation of both G_{49} and S_{53} to Leu or S_{53} and A_{57} to Leu resulted in a compounded reduction in signaling. Subsequent application of an operational model of receptor depletion (see Materials and methods) to the data yielded a value for P-factor affinity ($\log K_A = -7.0 \pm 0.16$). The model also enabled the determination of the relative efficacy ($\log \tau$) for the wildtype and receptor mutants as given in Table 1. The relative efficacy values were found to be significantly different from wildtype ($p < 0.01$) for the $Mam2^{S53L}$-GFP, $Mam2^{A57L}$-GFP, $Mam2^{G49L,S53L}$-GFP and $Mam2^{S53L,A57L}$-GFP mutants.

Table 1
Relative efficacy values ($\log \tau$) obtained for the wildtype Mam2 and Ste2 receptors and the receptor mutants in which the small-XXX-small motifs were disrupted (n = 3–5).

Mam2 Construct	log τ	Ste2 construct	Log τ
Mam2-GFP	0.89 ± 0.14	Ste2-GFP	1.58 ± 0.64
$Mam2^{G49L}$-GFP	0.06 ± 0.03		
$Mam2^{S53L}$-GFP	−0.15 ± 0.04	$Ste2^{G56L}$-GFP	−0.71 ± 0.33
$Mam2^{A57L}$-GFP	−0.11 ± 0.04	$Ste2^{G60L}$-GFP	−0.84 ± 0.37
$Mam2^{G49L,S53L}$-GFP	−0.67 ± 0.16	$Ste2^{G56L,G60L}$-GFP	−1.16 ± 0.49
$Mam2^{S53L,A57L}$-GFP	−0.59 ± 0.13		

Our molecular modeling also suggested that, in addition to the small-*XXX*-small motif, Q_{55} in TMD 1 of Mam2 may also be a site of TM helix interactions. In Ste2, the equivalent residue (R_{58}) has been shown to form part of the ligand-binding domain [49], and mutation of this residue severely attenuated ligand-binding (although membrane localization was not investigated). Analogous to the Ste2 data, we have previously identified a mutation of this residue, $Mam2^{Q55L}$, during a random mutagenic screen for inactive mutants and constitutive mutants of Mam2 [50]. $Mam2^{Q55L}$ was unable to induce any significant response within cells (E_{max}: Mam2 = 22.23 ± 0.77; $Mam2^{Q55L} = 0$).

To further explore the role of Q_{55}, we used our sequence alignments of TMD 1 given in Fig. 2G to map the small-*XXX*-small-*XXX*-small motif onto the opsin dimer (Fig. 5). Of the current crystal structures available, only the opsin dimer showed good alignment of the small-*XXX*-small motif although only the first residue (A_{41}) is small in rhodopsin. These residues (A_{42}, L_{47}, L_{50}, shown as spheres colored by atom type in Fig. 5A and B) nevertheless mediate the dimeric interaction in the opsin dimer. The opsin residue I_{48}, analogous in position to the Mam2 Q_{55} residue and shown in pink in Fig. 5A and B, is facing inwardly and strongly interacts with TM2. This suggests that the Q_{55} residue in Mam2 is similarly positioned and thus unable to perform any significant role in mediating the dimer interaction. Therefore, this mutation was not explored further.

To compare the effects of homologous mutations on Ste2 function using our assay, and compare our results to existing literature in this area, we first needed to establish that Ste2 could be functionally expressed in *S. pombe*. Although we have previously described the ability to heterologously express GPCRs from mammalian cells in *S. pombe* [20,21], we had not (until now) expressed the Ste2 from *S. cerevisiae*. Overall Mam2 and Ste2 share very little sequence homology (16.7% — EMBOSS Needle) [51], however this value increases to near

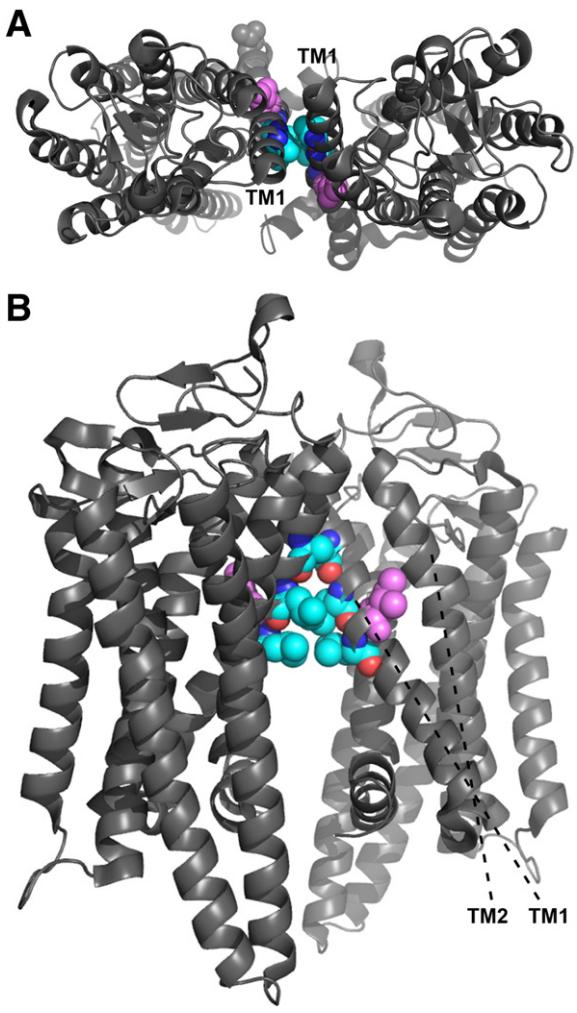

Fig. 5. Molecular modeling of the Mam2 using the opsin dimer. Two views of the opsin dimer (PDB ID 3CAP) with the small-XXX-small-XXX-small motif mapped onto A_{41}, L_{45} and L_{49} of TMD1 (shown as spheres and colored by atom type) in of the rhodopsin sequence in accordance with the alignment in Fig. 2G. TMD 1 is the major component of the interface. Ile_{48} (shown as spheres and colored pink), which corresponds to the position of R_{58} in Ste2 and Q_{55} in Mam2, is predicted to interact with TMD 2.

70% when only TMD 5, TMD 6 and TMD 7 are aligned. Given this level of homology between Mam2 and Ste2 it was not a surprise to observe that wild-type Ste2 could be functionally expressed in *S. pombe* when stimulated with its natural ligand α-factor (Fig. 4B). Comparison of each receptor's sensitivity to its respective pheromone suggested that Ste2 functioned equivalently to Mam2 in *S. pombe* (pEC_{50}: Ste2 − 7.87 ± 0.11; Mam2 − 7.88 ± 0.13). The mutant Ste2 receptors, in which the G_{56}-*XXX*-G_{60} motif was mutated to Leu, rendered *S. pombe* cells unable to respond to pheromone (Fig. 4B) and is in broad agreement with previous reports [12]. In contrast to Mam2, each individual mutation completely abolished the pheromone response indicating mechanistic differences between the receptors. Again application of the operational model for receptor depletion to the data yielded the α-factor affinity ($\log K_A = -6.22 \pm 0.60$) and the relative efficacy for each construct (Table 1). As observed for Mam2, the values for all three Ste2 mutants were found to be significantly different from the wildtype Ste2 ($p < 0.01$).

2.5. Mam2 trafficking disrupted upon mutation of small-XXX-small motifs

Given the previous reports that Ste2 receptors containing mutations in the small-*XXX*-small motif are not targeted correctly to the plasma membrane [12], and due to the similarity in the signaling properties of mutant Ste2 and Mam2 receptors, the subcellular distribution of all Mam2 (and Ste2, for comparison) mutants was investigated using confocal microscopy. Each mutant was generated as a C-terminal in-frame fusion to GFP and expressed from the pREP3x vector in the yeast strain JY1169 (Fig. 4C). To provide a robust measure of the subcellular distribution of the receptor mutants we utilized the QuimP2 plugin of ImageJ [40] as a quantitative measure of the fluorescence at the periphery of cells (Table S2). Whereas wild-type Mam2-GFP localized to the plasma membrane, the mutants appeared to localize to intracellular structures (Fig. 4C) [20]. Quantification of the peripheral membrane localization indicated that the $Mam2^{S53L}$, $Mam2^{A57L}$ and $Mam2^{G49L,S53L}$ and $Mam2^{S53L,A57L}$ mutants all display severely reduced plasma membrane localization (Fig. 4D–Table S2). The extent of the reduction in plasma membrane expression directly paralleled the reduction in signaling observed for these mutants. A similar trend was observed for the Ste2 small-*XXX*-small motif mutants where conversion of either glycine residue to leucine reduced plasma membrane expression between 4 and 10-fold (Fig. 4C and D–Table S2), with this reduction in expression directly mirrored in the reduced signaling characteristics. Correcting the signaling response (analogous to the method used in Weston et al. [38]) to account for reduced membrane expression of both Mam2 (Fig. 4F) and Ste2 (Fig. 4G) revealed that all mutant receptors were functional although only the Mam2 mutants displayed significant ($p < 0.01$) reduction in their potency (pEC_{50}: Mam2-GFP − 7.79 ±0.12; $Mam2^{S53L}$-GFP − 7.21 ± 0.10, $Mam2^{S53L}$-GFP − 6.71 ± 0.08, $Mam2^{A57L}$-GFP − 6.63 ± 0.06, $Mam2^{G49L,S53L}$-GFP − 7.00 ± 0.08 and $Mam2^{S53L,A57L}$-GFP

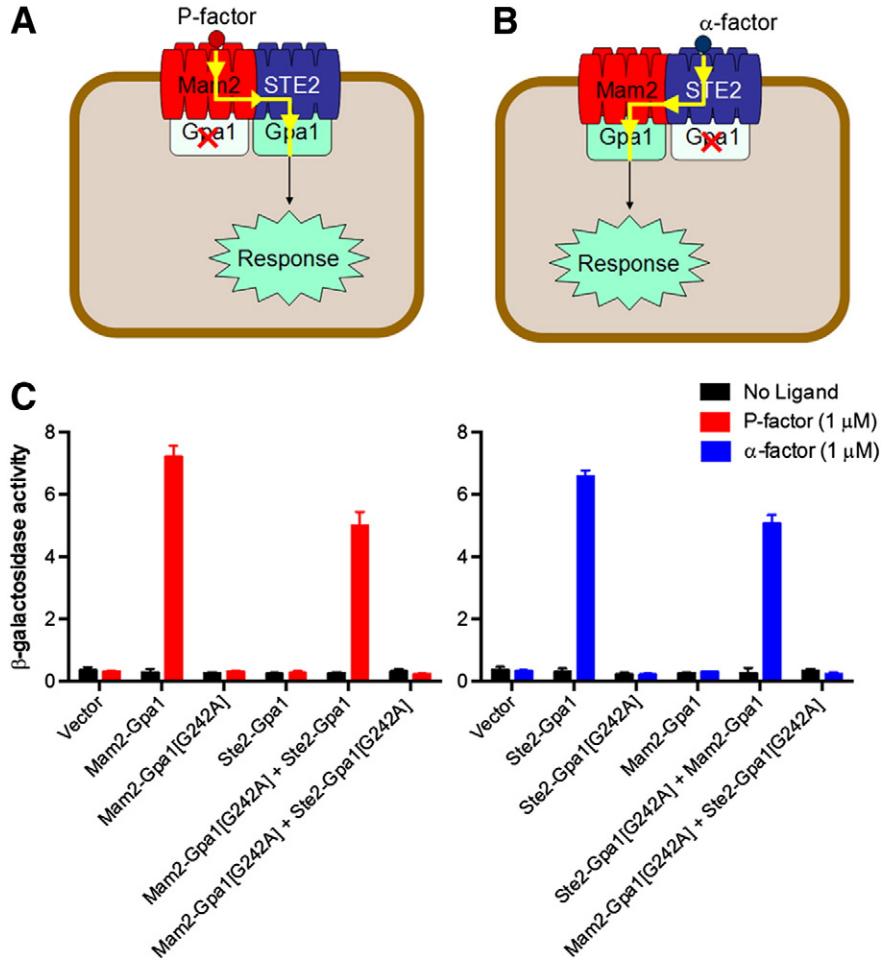

Fig. 6. Trans-activation enables functional characterization of a heterodimer between Mam2 and Ste2. Trans-activation requires the co-expression of two receptors; a functional receptor fused to an inactive Gα-subunit, and an inactive receptor fused to an active Gα-subunit. To demonstrate the functional heterodimerization of Mam2 and STE2 A) Mam2-Gpa1[G243A] and STE2-Gpa1 or B) Mam2-Gpa1 and STE2-Gpa1[G243A] were co-expressed and responses were measured using the β-galactosidase assay. C) Constructs as shown expressed in the *S. pombe* cells lacking both Mam2 and Gpa1 (JY1241). Activities were measured using the β-galactosidase assay in response to stimulation with no ligand, 1 μM P-factor or 1 μM α-factor. Means of triplicate results + SEM are shown.

− 6.76 ± 0.04). These data would suggest that mutation of the small-*XXX*-small motif of Mam2 specifically affects receptor trafficking and functionality while for Ste2 it appears to only affect plasma membrane translocation.

2.6. Cross-talk between Mam2 and Ste2 is mediated via small-XXX-small interactions

The presence of complementary small-*XXX*-small motifs in the first TMD of both Mam2 and Ste2, motifs which have been shown to facilitate both homo- and hetero-association of membrane-embedded α-helices [52,53], led us to investigate whether a functional interaction might occur between these two receptors. We have previously described the use of GPCR-Gpa1 fusion constructs to investigate Mam2 dimerization through the principle of GPCR *trans*-activation [20]. Briefly, a receptor of choice is fused directly-in frame to an active Gpa1 or a mutant of Gpa1[G234A] that is unable to displace GDP [20]. Then by using the principle described in Fig. 6A and B we are able to express combinations of the Mam2 and Ste2 fusion constructs to determine if these receptors generate functional heterodimers. Co-expression of Mam2-Gpa1[G243A] with Ste2-Gpa1 (in cells lacking endogenous Mam2 and Gpa1) following stimulation with 1 μM P-factor was able to generate a signaling response (Fig. 6C). Given that Mam2 fused to the inactive Gpa1 (Mam2-Gpa1[G243A]) fails to elicit a response upon stimulation with P-factor, we would suggest that transactivation of response occurs from the ligand-occupied Mam2 to the functional Gpa1 fused onto Ste2. We have shown previously that Mam2-Gpa1[G243A] is unable to activate Gpa1 in the absence of the formation of a dimer [20]. Consequently we suggest that the two related fungal GPCRs can form a functional dimer pair. The converse situation also applied when Ste2-Gpa1 [G243A] was co-expressed with Mam2-Gpa1 and stimulated with 1 μM α-factor.

We next sought to determine if this heterodimer between Ste2 and Mam2 displayed any unique pharmacological properties. To achieve this, we made use of a series of *S. pombe* Gα-transplant reporter strains [21]. While these strains are generally used to investigate the Gα-specificity of human GPCRs, [7] we have previously used these strains to investigate the profile of Gα-transplants activated by Mam2 [20]. In our current study we not only investigated the Gα-specificity of Mam2 in these Gα-transplant reporter strains (Fig. 7A) but also extended these studies to include Ste2 (Fig. 7B). Consistent with our previous analyses, we observed that Mam2, when stimulated with 1 μM P-factor, activated the $G_{\alpha q}$ and $G_{\alpha 16}$ transplants to a similar extent as Gpa1, while the $G_{\alpha i3}$ transplant displayed a reduced but significant level of response. In contrast to our previous study, we did not observe a significant response from the $G_{\alpha i2}$ transplant strain, and this may reflect a difference in the extent of receptor expression between the two studies. Here we are using the pREP4x plasmid to drive Mam2 expression (enabling co-expressing with Ste2 as described below) and this may produce a lower level of expression than the pREP3x vector used in our previous

study [21]. To facilitate immunoblotting to confirm the expression of the Mam2, we expressed the C-terminal fusion of Mam2 tagged with GFP (Fig. 7A). Membrane extracts generated from the $G_{\alpha i3}$ transplant strain confirmed the expression of Mam2-GFP and also highlighted the existence of higher order oligomeric states (see Fig. 7A, inset). As we have described previously [20] a smaller species of about 30 kDa was also observed which we attributed to being a breakdown product of Mam2-GFP.

Using a similar approach, the profile of Gα-transplant reporter strains activated by Ste2 was investigated in response to 1 μM α-factor (Fig. 7B). Comparable to Mam2, when Ste2 was stimulated by its endogenous ligand (α-factor), the $G_{\alpha q}$ and $G_{\alpha 16}$ transplant strains were activated to an equivalent extent as the endogenous Gpa1 strain. Unlike Mam2, Ste2 was unable to stimulate the $G_{\alpha i3}$ transplant strain despite showing good expression and the existence of high order oligomeric states (when analyzed using a hexahistidine tag under non-reducing conditions, Fig. 7B, inset). Ste2 has previously been demonstrated to be N-terminally glycosylated on two sites [54] and hence the existence of multiple bands for the monomer and dimer states. The inability of Ste2 to activate a yeast/human $G_{\alpha i3}$ transplant in *S. pombe* is entirely consistent with that reported when similar chimeras have been expressed in *S. cerevisiae* [55]. Moreover, to ensure the highest level of expression possible of Ste2 we have used the pREP3x vector with cells grown in the absence of thiamine.

These results show distinctive G protein activation profiles for Mam2 and Ste2 in response to their native ligands. To determine if Mam2 and Ste2 could form a functional complex, we co-expressed the two receptors in the Gα-transplant reporter strains and stimulated the cells with either 1 μM P-factor or 1 μM α-factor (Fig. 7C). In response to P-factor stimulation, the activation profile of the co-expressed receptors resembled that of Mam2 expressed alone, but with a reduced overall level of signaling, possibly due to Ste2 sequestering some of the Gα pool. When the same strains were stimulated with α-factor, we observed an activation profile consistent with that observed for Ste2 alone, but with the additional activation of the $G_{\alpha i3}$ transplant. This transplant was not activated when Ste2 was expressed alone, and suggests that Mam2 influences the Gα specificity of Ste2 in response to α-factor. Furthermore, immunoblotting (using non-reducing conditions) of plasma membrane extracts isolated from the G_{i3} transplant strain (Fig. 7C, insets) against His_6 revealed the presence of a species that did not correspond to Ste2-His_6 alone. To confirm that this new band was not simply due to differential sample loading in the two blots, a loading control was run for each and is shown in Fig. S3. This new species was approximately 15 kDa larger than the predicted size for a Ste2-His_6 homo-dimer and was the correct size expected for a heterodimer of Ste2-His_6 with Mam2-GFP.

Having established the potential for Ste2 and Mam2 to form a functional complex, we sought to determine if the small-*XXX*-small motifs present in TMD 1 of both receptors facilitated this interaction. We have reported that the trafficking and activities of Mam2^{G49L,S53L} and Ste2 ^{G56L,G60L} were severely affected compared to their respective wild-type receptors (Fig. 4A–B) when expressed individually. We therefore wondered if co-expression of a wildtype receptor with a mutant receptor would overcome the trafficking and activities' defects. To facilitate a clear distinction between the mutant and wildtype receptor we used the ability of Mam2 to dimerize with Ste2 as our functional readout. Therefore we co-expressed mutant receptors with wildtype partners and investigated the Gα-specificity profiles (Fig. 8). The

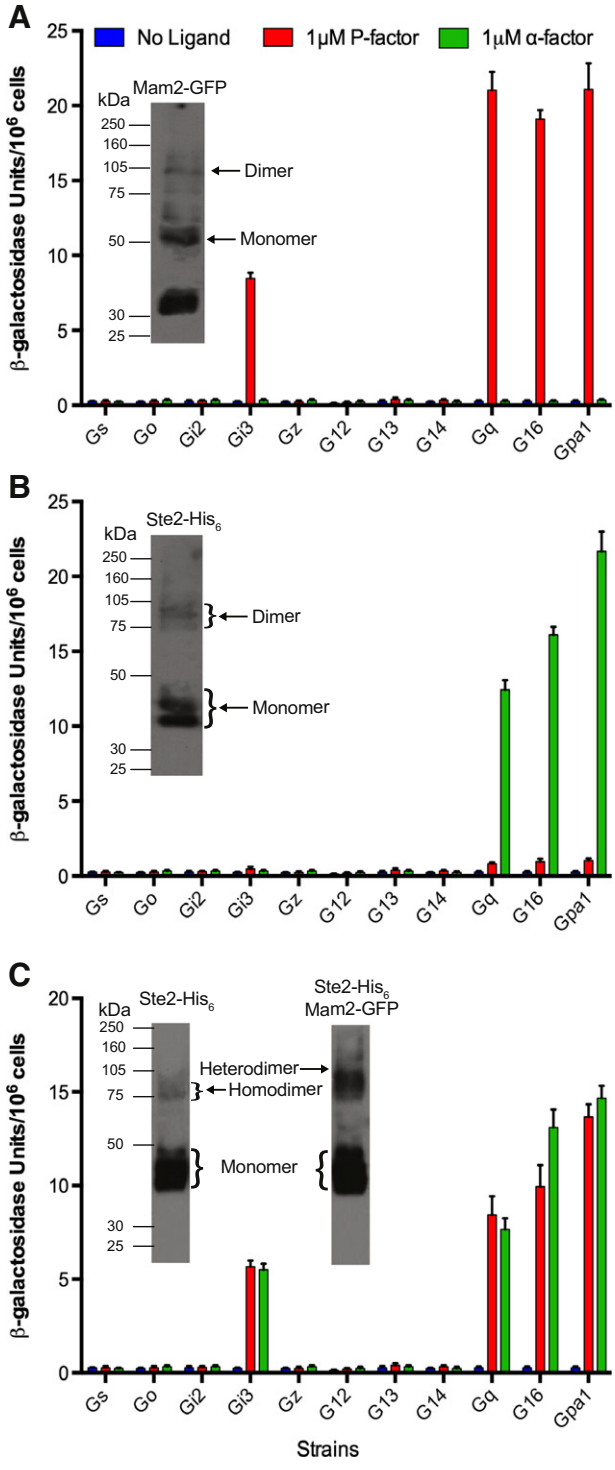

Fig. 7. Heterodimer of Mam2 and Ste2 displays altered G protein selectivity compared to the homodimers. A series of *S. pombe* reporter strains containing a different Gα-transplant but all lacking Mam2, was transformed with (A) pREP4x-Mam2, (B) pREP3x-Ste2, and (C) both pREP4x-Mam2 and pREP3x-Ste2. Cells were grown in the absence of thiamine to induce full expression from the *nmt1* promoter and production of β-galactosidase from each Gα-transplant strain was assayed using ONPG as a substrate. (A) Cells expressing Mam2 were exposed to no ligand (blue columns), 1 μM P-factor (red columns) or 1 μM α-factor (green columns) for 16 h and β-galactosidase production assayed. Mam2-GFP expression was confirmed by immunoblotting of plasma membrane extracts (10 mg) prepared from the $G_{\alpha i3}$ transplant strain. Samples were separated by non-reducing SDS-PAGE, and western blots were probed using a rabbit GFP monoclonal antibody. Indicated are sizes for monomeric Mam2-GFP and the putative dimer (100 kDa). A smaller band of 30 kDa was observed and has been previously suggested to be a breakdown product of Mam2-GFP. (B) Cells expressing Ste2 were assayed as in A. Ste2-His_6 expression was confirmed by immunoblotting of plasma membrane extracts (10 mg) prepared from the Gi3 transplant strain using a rabbit polyclonal anti-6-His antibody. Indicated are sizes for monomeric Ste2-His_6 and the putative dimer. (C) Cells co-expressing Mam2 and Ste2 were assayed as in A. Membrane extracts were generated from the $G_{\alpha i3}$ transplant strains and probed using a rabbit polyclonal anti-6-His antibody only. Indicated are sizes for monomeric Ste2-His_6 and the Mam2-GFP/Ste2-His_6 dimer. Results are means ± S.E.M. for triplicate measurements from three independent isolates.

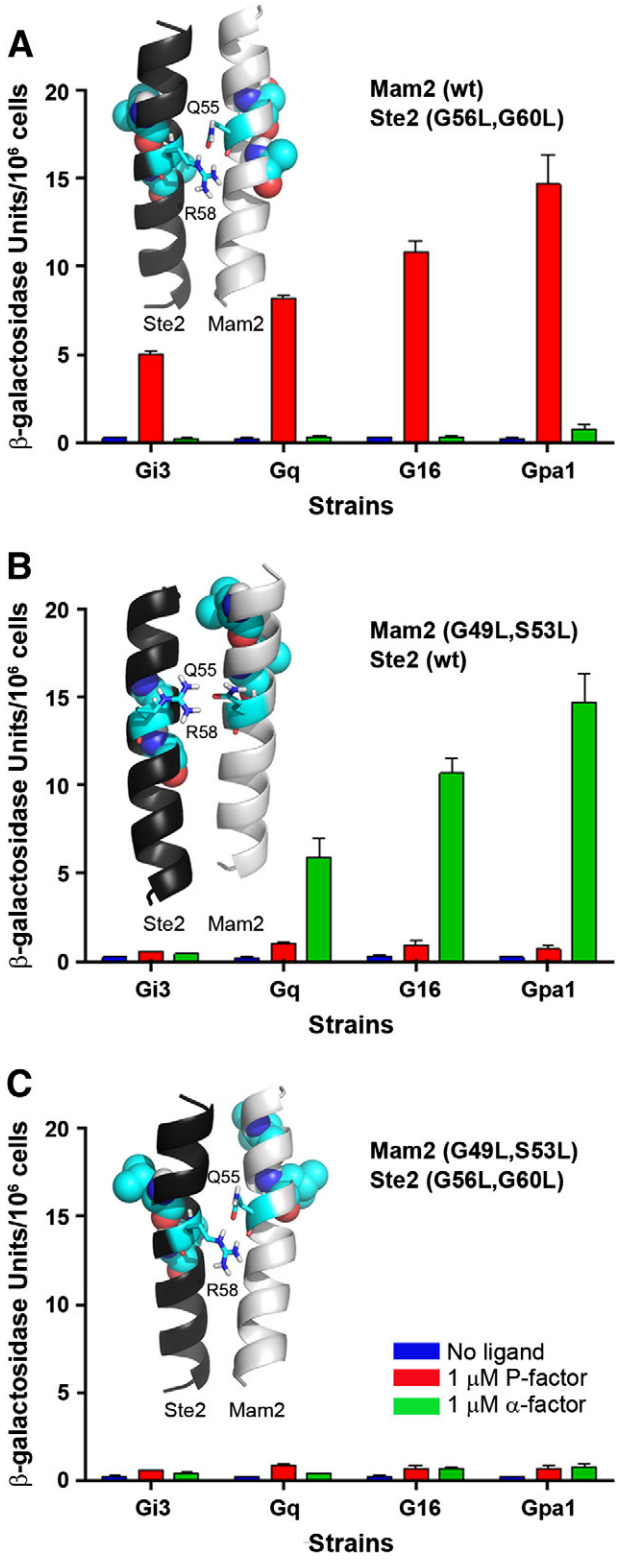

Fig. 8. Effect of small-XXX-small mutants on Mam2-Ste2 hetero-association. The strains JY1160 (expressing the G_{i3} transplant), JY1165 (G_q), JY1167 (G_{16}) and JY1169 (Gpa1) were transformed with (A) pREP4x-Mam2 & pREP3x-Ste2$_{(G56L,G60L)}$, (B) pREP4x-Mam2$_{(G49L,S53L)}$ & pREP3x-Ste2 and (C) pREP4x-Mam2$_{(G49L,S53L)}$ & pREP3x-Ste2$_{(G56L,G60L)}$. Cells were grown in the absence of thiamine to induce full expression from the *nmt1* promoter and production of β-galactosidase from each Gα-transplant strain in response to stimulation with no ligand, 1 μM P-factor and 1 μM α-factor was assayed using ONPG as substrate. Results are means ± S.E.M. for triplicate measurements from three independent isolates. Insets from panels (A–C) are molecular models obtained from searches of the corresponding mutant hetero-dimer. The predominant structure observed in all three cases is a dimer stabilized by a pair of polar residues (small-XXX-small motifs or their mutants, shown in space filling representation, are excluded from the interface).

activation profile upon addition of 1 μM P-factor for Gα-transplant strains expressing wildtype Mam2 and Ste2^{G56L,G60L} was reminiscent of that for Mam2 expressed alone (Fig. 8A). In contrast, 1 μM α-factor induced a minimal response in Gα-transplant strains. This suggests that Mam2–Ste2 interactions were disrupted, and the responses observed were predominantly from Mam2. The reverse configuration of receptors, Mam2^{G49L,S53L} and wildtype Ste2 (Fig. 8B), gave a similar activation profile to Ste2 alone in response to α-factor stimulation, except that the maximal level of signaling was reduced when co-expressed with Mam2^{G49L,S53L}. Co-expression of Mam2^{G49L,S53L} and Ste2^{G56L,G60L} (Fig. 8C) yielded a limited response to P-factor in the $G_{\alpha i3}$, $G_{\alpha q}$ and $G_{\alpha 16}$ transplant strains, and Gpa1 in response to either pheromone, but no signaling through $G_{\alpha i3}$ was observed when the cells were stimulated with α-factor suggesting abolishment of any interaction between the two receptors. Together, these data suggest a role for the conserved TMD 1 small-*XXX*-small motifs in hetero-association of Mam2 and Ste2. Moreover, co-expression of wildtype receptors with mutants displaying trafficking and functional defects could not restore functionality to the mutants.

Computational models (created using CHI as before) of Ste2-Mam2 TMD 1 hetero-dimers support these results. Structures containing the Mam2 S-*XXX*-A and the Ste2 G-*XXX*-G motifs packed at the heterodimer interface were reproducibly found (see Fig. 3G for a representative structure), illustrating how these two GPCRs could interact via complementary small-*XXX*-small motifs located in TMD 1. Two additional types of interactions were also found at the heterodimer interface: (i) the Mam2 S-*XXX*-A motif close-packing against an alternative helical face of Ste2 TMD 1 (Fig. 3H); (ii) Q_{55} in Mam2 forming an interhelical H-bond with R_{58} in Ste2 (Fig. 3I). These interactions were not investigated further (e.g. via mutagenesis) here. To simulate the impact of introducing Leu residues into the heterodimer interface, the mutants described in Fig. 8 were translated into molecular models and CHI searches were again used to probe low energy configurations. In all three cases, mutation of small-*XXX*-small motifs at the proposed heterodimer interface overwhelmingly yielded heterodimers that favored interhelical H-bond formation between Q_{55} from Mam2 and R_{58} from Ste2. Typical structures for the appropriate TMD pair are shown in Fig. 8D–F, and resemble an arrangement also observed for wild-type (Fig. 3I). This would suggest that, in the absence of complementary small-*XXX*-small motifs, the most favorable interaction for the isolated TM domains is that between Q_{55} and R_{58}. Given the overwhelming experimental support for the role of small-*XXX*-small motifs in this work, the fact that interaction of Q_{55}/R_{58} would require a ~180° rotation of the TMD 1 helices from their small-*XXX*-small-containing faces, and the previous report that in Ste2 R_{58} forms part of the ligand binding site [49], it seems unlikely that the hetero-interaction could be accommodated via both types of interactions. However, more work is required to confirm this.

3. Discussion

Recently, the accumulation of pharmacological and biochemical data has significantly challenged the notion that GPCRs act as monomers [56–60] transducing signals to a heterotrimeric G protein, although this is not without controversy. Some of the early evidence for GPCR dimerization came from unexplained cooperativity observed in ligand binding assays and abnormally large receptor complexes observed using gel filtration [61–63]. Oligomerization of GPCRs was originally centered upon receptor self-association (homo-dimerization), with studies of the fungal GPCRs Ste2 [10,12] and Mam2 [21] playing significant roles. There is now an ever-increasing list of receptors that have been suggested to associate with other GPCRs (hetero-dimerization), and many of these examples have been summarized in an excellent recent review [64]. However, certain concerns remain in the field that these interactions are due to experimental artifacts. For example, frequently GPCRs are overexpressed in a given assay system or contain large fluorescent moieties that themselves promote oligomerization.

Two particularly favored methods to determine GPCR hetero-dimerization are FRET and BRET techniques, however these methods often require removal of the C-terminal intracellular tail of the receptor to enable fluorophores to come into close proximity and create a signal [10,12]. Where such studies are coupled to functional data, the case for hetero-dimerization is more compelling. GPCR hetero-dimerization may also be responsible for efficient trafficking of receptors to the plasma membrane, with a clear example being the $GABA_B$ receptor. To enable cell surface expression of a functional $GABA_B$ receptor, two distinct but related GPCRs ($GABA_BR1$ and $GABA_BR2$) must be co-expressed in cells [65]. More recent work has shown that classical Family A receptors such as the β-adrenergic receptors [66–68] can also undergo hetero-dimerization. However, despite multiple examples, the mechanisms used by receptors to promote oligomerization are not clearly understood.

Here we present an array of biochemical, computational and cellular data demonstrating for the first time that a highly conserved small-*XXX*-small motif found in TMD 1 of the fungal GPCR Mam2 promotes TMD 1 self-association. We provide molecular models for these interactions that are chemically plausible and in very good agreement with experiment. Given the potential importance of dimerization on efficient GPCR plasma membrane trafficking, we investigated the effects of perturbations of the small-*XXX*-small motif in Mam2 in vivo. Consistent with our predictions, and with results obtained in parallel for the homologous GPCR Ste2, disruption of the close packing of the TMD 1 motif reduced the ability of both receptors to respond to their native pheromones, and resulted in impaired plasma membrane expression.

3.1. GPCR dimerization interfaces

Oligomerization of some GPCRs appears to be mediated by extracellular regions, for instance the metabotropic glutamate receptors dimerize via disulphide bond formation [69] and dimerization of the CXCR4 receptor appears to be driven by the hydrophobic effect involving the extracellular regions of TMDs 5 and 6 [70]. Oligomerization driven by interactions formed in the TM bundle is also poorly characterized in the literature, but small-*XXX*-small motifs have been implicated. For instance, a G-*XXX*-G motif drives the oligomerization of the beta2-adrenergic receptor [71] and, as discussed in this work, contributes to the oligomerization of the *S. cerevisiae* Ste2 pheromone GPCR [10,12]. Interestingly the beta2-adrenergic receptor appears to be an isolated case since the small-*XXX*-small in TM6 is not conserved in Family A GPCRs [36].

Although a G-*XXX*-G motif in TMD 1 of Ste2 has been highlighted in homo-oligomer formation, we present data here which indicate, surprisingly, that Ste2 TMD 1 only weakly self-associates in isolation in a natural membrane (albeit a bacterial membrane) and is unlikely to single-handedly direct oligomerization outside the context of the full-length receptor. This would suggest one of two things, either (a) that TMD 1 does not participate in intermolecular interactions but instead stabilizes intramolecular contacts that lead to the correct folding of the protein, or (b) that TMD 1 works in concert with other regions of the protein to facilitate intermolecular interactions. In a Ste2 homo-dimer, for example, more than one TMD could be in contact at one time depending on the arrangement of the proteins in the dimer. Indeed, the N-terminus, TMD 2, TMD 4, and TMD 7 of Ste2 have also been implicated in direct protein-protein interactions [9–11], while the opsin dimer (Fig. 5) is held together by additional contacts within TMD 2 and helix 8.

Similar to Ste2, the orthologous *S. pombe* pheromone receptor Mam2 also contains a motif of small residues (S-*XXX*-A) at the same position in TMD 1 (indeed this motif is conserved through several members of Class D GPCRs, see Fig. 2) and also forms homo-oligomeric complexes [20]. In contrast to Ste2, we show that Mam2 TMD 1 strongly self-associates in a natural membrane in a sequence dependent manner via the S-*XXX*-A motif suggesting that Mam2 TMD 1 may be capable of driving self-association of the receptor. Despite these differences in the mechanism of self-association of the two GPCRs, mutation of the complementary small-*XXX*-small motifs found in TMD 1 had a similar impact on the function and localization of both proteins. Substitution of the small Ala, Ser or Gly residues with Leu severely impaired the pheromone response of both proteins and greatly reduced the plasma membrane expression levels (receptors were instead found in intracellular compartments) suggesting inefficient folding of the GPCRs.

3.2. Functional hetero-dimerization of fungal GPCRs

The fungal GPCRs constitute the fourth family of GPCRs (class D — fungal mating pheromone receptors) and display little significant inter-species sequence conservation. For example, the two-pheromone receptors from *S. cerevisiae* (Ste2 and Ste3) only share 15% homology, consequently the receptors have been given their own unique 7 TM classification. Between species however, the receptors are more homologous (Mam2 and Ste2 share 70% homology over the TMDs 5, 6 and 7). While it is highly unlikely that intra-species fungal GPCR dimerization would functionally occur, there have been reports that during cell fusion Ste2 and Ste3 may form a dimeric complex that mediates cell wall digestion and membrane juxtaposition before fusion [72]. Despite this report, no information is available relating to the potential dimeric interface between Ste2 and Ste3. Further, based upon our alignments, Ste3 would appear not to have a conserved small-*XXX*-small motif and indeed may resemble more the traditional small-*XX*-small motif of Family A GPCRs (Reynolds et al., unpublished work). The only other descriptions to date of fungal GPCR heterodimerization relates to the use of artificially expressed constitutive and dominant negative versions of receptors [20,73,74]. Our ability to functionally express the *S. cerevisiae* pheromone receptor Ste2 in *S. pombe* has enabled us to demonstrate here, for the first time, the propensity of highly related yet species-distinct GPCRs Ste2 and Mam2 to form hetero-dimers. Their structural and functional similarity, and the complementary positioning of a well-studied helix–helix interaction motif, suggested the possibility of the formation of a functional heterodimer. This was confirmed through the use of previously described *S. pombe* Gα-transplant strains [21] and immunoblotting. Perturbation of the small-*XXX*-small motif in either receptor abolished functional heterodimer formation.

3.3. Implications beyond yeast

The data presented in this study highlight the wide array of in vitro and in vivo techniques available for the investigation of GPCR oligomerization, as well as the potential of small-*XXX*-small motifs to promote interactions and facilitate correct membrane trafficking in this context. While biologically our identification of a functional heterodimeric complex between two GPCRs from different yeast species (Ste2 and Mam2) is unlikely to occur in nature, it does highlight the potential for related GPCRs with homology between their TMDs to associate. Physiologically, an interaction between Ste2 and Mam2 will not occur, however given their structural similarities they represent an excellent model to study hetero-dimerization of related-GPCRs without the complication of competing ligands. Given that a number of mammalian GPCRs contain the small-*XXX*-small motif in their TMDs [10], some of which have been demonstrated to promote oligomerization (e.g. the beta2-adrenergic receptor [71]) even though the motif is not conserved in the class as a whole, it will be of great interest to determine if any of these facilitate functional homo-dimer and hetero-dimer couplings.

Acknowledgements

A.M.D. would like to acknowledge the use of computing facilities at the University of Warwick Centre for Scientific Computing.

Appendix A. Supplementary data

Alignment of full-length Ste2 and Mam2, western blots to measure expression levels of all TOXCAT constructs used in this study, and loading controls are provided, so are tables listing all *Schizosaccharomyces pombe* strains used in this study, peripheral membrane intensities and percentage mean fluorescence values for Mam2 and Ste2 mutants. Supplementary data to this article can be found online at http://dx.doi.org/10.1016/j.bbamem.2014.08.019.

References

[1] S.G. Rasmussen, B.T. DeVree, Y. Zou, A.C. Kruse, K.Y. Chung, T.S. Kobilka, F.S. Thian, P.S. Chae, E. Pardon, D. Calinski, J.M. Mathiesen, S.T. Shah, J.A. Lyons, M. Caffrey, S. H. Gellman, J. Steyaert, G. Skiniotis, W. Weis, R.K. Sunahara, B.K. Kobilka, Crystal structure of the β2 adrenergic receptor–Gs protein complex, Nature 477 (2011) 549–555.

[2] F. Xu, H. Wu, V. Katritch, G.W. Han, K.A. Jacobson, Z.G. Gao, V. Cherezov, R.C. Stevens, Structure of an agonist-bound human A2A adenosine receptor, Science 332 (2011) 322–327.

[3] S. Terrillon, M. Bouvier, Roles of G-protein-coupled receptor dimerization, EMBO Rep. 5 (2004) 30–34.

[4] R.J. Ward, T.R. Xu, G. Milligan, GPCR oligomerization and receptor trafficking, Methods Enzymol. 521 (2013) 69–90.

[5] F.M. Décaillot, M.A. Kazmi, Y. Lin, S. Ray-Saha, T.P. Sakmar, P. Sachdev, CXCR7/CXCR4 heterodimer constitutively recruits beta-arrestin to enhance cell migration, J. Biol. Chem. 286 (2011) 32188–32197.

[6] P. Chandrasekera, T. Wan, E. Gizewski, J. Auchampach, R. Lasley, Adenosine A(1) receptors heterodimerize with beta(1)- and beta(2)-adrenergic receptors creating novel receptor complexes with altered G protein coupling and signaling, Cell. Signal. 25 (2013) 736–742.

[7] G. Ladds, J. Davey, Analysis of human GPCRs in fission yeast, Curr. Opin. Drug Discov. Dev. 7 (2004) 683–691.

[8] A.U. Gehret, A. Bajaj, F. Naider, M.E. Dumont, Oligomerization of the yeast alpha-factor receptor: implications for dominant negative effects of mutant receptors, J. Biol. Chem. 281 (2006) 20698–20714.

[9] H. Kim, B.K. Lee, F. Naider, J.M. Becker, Identification of specific transmembrane residues and ligand-induced interface changes involved in homo-dimer formation of a yeast G protein-coupled receptor, Biochemistry 48 (2009) 10976–10987.

[10] M.C. Overton, K.J. Blumer, The extracellular N-terminal domain and transmembrane domains 1 and 2 mediate oligomerization of a yeast G protein-coupled receptor, J. Biol. Chem. 277 (2002) 41463–41472.

[11] H.X. Wang, J.B. Konopka, Identification of amino acids at two dimer interface regions of the alpha-factor receptor (Ste2), Biochemistry 48 (2009) 7132–7139.

[12] M.C. Overton, S.L. Chinault, K.J. Blumer, Oligomerization, biogenesis, and signaling is promoted by a Glycophorin A-like dimerization motif in transmembrane domain 1 of a yeast G protein-coupled receptor, J. Biol. Chem. 278 (2003) 49369–49377.

[13] B. Brosig, D. Langosch, The dimerization motif of the glycophorin A transmembrane segment in membranes: importance of glycine residues, Prot. Sci. 7 (1998) 1052–1056.

[14] Z.A. Jenei, K. Borthwick, V.A. Zammit, A.M. Dixon, Self-association of transmembrane domain 2 (TM2), but not TM1, in carnitine palmitoyltransferase 1A: role of GXXXG(A) motifs, J. Biol. Chem. 284 (2009) 6988–6997.

[15] A. Rath, C.M. Deber, Surface recognition elements of membrane protein oligomerization, Proteins 70 (2008) 786–793.

[16] D. Gerber, N. Sal-Man, Y. Shai, Two motifs within a transmembrane domain, one for homodimerization and the other for heterodimerization, J. Biol. Chem. 279 (2004) 21177–21182.

[17] F. Cunningham, B. Poulsen, W. Ip, C. Deber, Beta-branched residues adjacent to GG4 motifs promote the efficient association of glycophorin A transmembrane helices, Biopolymers 96 (2011) 340–347.

[18] A. Doura, F. Kobus, L. Dubrovsky, E. Hibbard, K. Fleming, Sequence context modulates the stability of a GxxxG-mediated transmembrane helix–helix dimer, J. Mol. Biol. 341 (2004) 991–998.

[19] K. Kitamura, C. Shimoda, The *Schizosaccharomyces-pombe* Mam2 gene encodes a putative pheromone receptor which has a significant homology with the saccharomyces-cerevisiae Ste2 protein, EMBO J. 10 (1991) 3743–3751.

[20] G. Ladds, K. Davis, A. Das, J. Davey, A constitutively active GPCR retains its G protein specificity and the ability to form dimers, Mol. Microbiol. 55 (2005) 482–497.

[21] G. Ladds, K. Davis, E.W. Hillhouse, J. Davey, Modified yeast cells to investigate the coupling of G protein-coupled receptors to specific G proteins, Mol. Microbiol. 47 (2003) 781–792.

[22] W. Croft, C. Hill, E. McCann, M. Bond, M. Esparza-Franco, J. Bennett, D. Rand, J. Davey, G.A. Ladds, A physiologically required G protein-coupled receptor (GPCR)-regulator of G protein signaling (RGS) interaction that compartmentalizes RGS activity, J. Biol. Chem. 288 (2013) 27327–27342.

[23] B. Smith, C. Hill, E. Godfrey, D. Rand, H. van den Berg, S. Thornton, M. Hodgkin, J. Davey, G.A. Ladds, Dual positive and negative regulation of GPCR signaling by GTP hydrolysis,, Cell. Signal. 21 (2009) 1151–1160.

[24] W.P. Russ, D.M. Engelman, TOXCAT: a measure of transmembrane helix association in a biological membrane, Proc. Natl. Acad. Sci. U. S. A. 96 (1999) 863–868.

[25] M.D. Abramoff, P.J. Magalhaes, S.J. Ram, Image processing with ImageJ, Biophoton. Int. 11 (2004) 36–42.

[26] J. Davey, R. Egel.,, O. Neilsen, Pheromone procedures in fission yeast, Methods Mol. Genet. 6 (1995) 247–263.

[27] G. Ladds, E.M. Rasmussen, T. Young, O. Nielsen, J., D., The sxa2-dependent inactivation of the P-factor matin pheromone in the fission yeast, Mol. Microbiol. 20 (1996) 35–42.

[28] K. Maundrell, Thiamine-repressible expression vectors pREP and pRIP for fission yeast, Gene 123 (1993) 127–130.

[29] M. Didmon, K. Davis, P. Watson, G. Ladds, P. Broad, J. Davey, Identifying regulators of pheromone signalling in the fission yeast *Schizosaccharomyces pombe*, Curr. Genet. 41 (2002) 241–253.

[30] P.D. Adams, D.M. Engelman, A.T. Brünger, Improved prediction for the structure of the dimeric transmembrane domain of glycophorin A obtained through global searching, Proteins 26 (1996) 257–261.

[31] A.P. Brünger AT, G.M. Clore, W.L. DeLano, P. Gros, R.W. Grosse-Kunstleve, J.S. Jiang, J. Kuszewski, M. Nilges, N.S. Pannu, R.J. Read, L.M. Rice, T. Simonson, G.L. Warren, Crystallography & NMR system: a new software suite for macromolecular structure determination, Acta Crystallogr. D Biol. Crystallogr. 54 (1998) 905–921.

[32] E. Krissinel, K. Henrick, Inference of macromolecular assemblies from crystalline state, J. Mol. Biol. 372 (2007) 774–797.

[33] L.M. Simpson, B. Taddese, I.D. Wall, C.A. Reynolds, Bioinformatics and molecular modelling approaches to GPCR oligomerization, Curr. Opin. Pharmacol. 10 (2010) 30–37.

[34] A. Krogh, B. Larsson, G. von Heijne, E.L. Sonnhammer, Predicting transmembrane protein topology with a hidden Markov model: application to complete genomes, J. Mol. Biol. 305 (2001) 567–580.

[35] B. Taddese, G.J. Upton, G.R. Bailey, S.R. Jordan, N.Y. Abdulla, P.J. Reeves, C.A. Reynolds, Do plants contain G protein-coupled receptors? Plant Physiol. 164 (2014) 287–307.

[36] S. Vohra, B. Taddese, A.C. Conner, D.R. Poyner, D.L. Hay, J. Barwell, P.J. Reeves, G.J. Upton, C.A. Reynolds, Similarity between class A and class B G-protein-coupled receptors exemplified through calcitonin gene-related peptide receptor modelling and mutagenesis studies, J R. Soc Interface 10 (2013) 20120846.

[37] J.H. Park, P. Scheerer, K.P. Hofmann, H.W. Choe, O.P. Ernst, Crystal structure of the ligand-free G-protein-coupled receptor opsin, Nature 454 (2008) 183–187.

[38] C. Weston, M. Bond, C. Croft, J. Davey, G. Ladds, The coordination of cell growth during fission yeast mating requires Ras1-GTP hydrolysis, PLoS ONE 8 (10) (2013) e77487.

[39] M. Bond, W. Croft, R. Tyson, T. Bretschneider, J. Davey, G. Ladds, Quantitative analysis of human ras localisation and function in the fission yeast *Schizosaccharomyces pombe*, Yeast 30 (2013) 145–156.

[40] L. Bosgraaf, P. van Haastert, T. Bretschneider, Analysis of cell movement by simultaneous quantification of local membrane displacement and fluorescent intensities using Quimp2, Cell Motil. Cytoskeleton 66 (2009) 156–165.

[41] D. Dormann, T. Libotte, C. Weijer, T. Bretschneider, Simultaneous quantification of cell motility and protein-membrane association using active contours, Cell Motil. Cytoskeleton 52 (2002) 221–230.

[42] J.W. Black, P. Leff, Operational models of pharmacological agonism, Proc. R. Soc. B Biol. Sci. 220 (1983) 141–162.

[43] M.A. Larkin, G. Blackshields, N.P. Brown, R. Chenna, P.A. McGettigan, H. McWilliam, F. Valentin, I.M. Wallace, A. Wilm, R. Lopez, J.D. Thompson, T.J. Gibson, D.G. Higgins, Clustal W and Clustal X version 2.0, Bioinformatics 23 (2007) 2947–2948.

[44] J.D. Thompson, T.J. Gibson, F. Plewniak, F. Jeanmougin, D.G. Higgins, The CLUSTAL_X windows interface: flexible strategies for multiple sequence alignment aided by quality analysis tools, Nucleic Acids Res. 25 (1997) 4876–4882.

[45] H. Wu, C. Wang, K.J. Gregory, G.W. Han, H.P. Cho, Y. Xia, C.M. Niswender, V. Katritch, J. Meiler, V. Cherezov, Structure of a class C GPCR metabotropic glutamate receptor 1 bound to an allosteric modulator, Science 344 (2014) 58–64.

[46] D. Langosch, B. Brosig, H. Kolmar, H.J. Fritz, Dimerisation of the glycophorin A transmembrane segment in membranes probed with the ToxR transcription activator, J. Mol. Biol. 263 (1996) 525–530.

[47] R.M. Johnson, A. Rath, C.M. Deber, The position of the Gly-xxx-Gly motif in transmembrane segments modulates dimer affinity, Biochem. Cell Biol. 84 (2006) 1006–1012.

[48] R. Li, R. Gorelik, V. Nanda, P.B. Law, J.D. Lear, W.F. DeGrado, J.S. Bennett, Dimerization of the transmembrane domain of Integrin alphaIIb subunit in cell membranes, J. Biol. Chem. 279 (2004) 26666–26673.

[49] C. Son, H. Sargsyan, F. Naider, J. Becker, Identification of ligand binding regions of the *Saccharomyces cerevisiae* alpha-factor pheromone receptor by photoaffinity cross-linking, Biochemistry 43 (2004) 13193–13203.

[50] A. Goddard, G. Ladds, R. Forfar, J. Davey, Identification of Gnr1p, a negative regulator of Got signalling in *Schizosaccharomyces pombe*, and its complementation by human G beta subunits, Fungal Genet. Biol. 43 (2006) 840–851.

[51] D.J. Lipman, W.R. Pearson, Rapid and sensitive protein similarity searches, Science 227 (1985) 1435–1441.

[52] G. King, A.M. Dixon, Evidence for role of transmembrane helix–helix interactions in the assembly of the class II major histocompatibility complex, Mol. BioSyst. 6 (2010) 1650–1661.

[53] Z.A. Jenei, G.Z. Warren, M. Hasan, V.A. Zammit, A.M. Dixon, Packing of transmembrane domain 2 of carnitine palmitoyltransferase-1A affects oligomerization and malonyl-CoA sensitivity of the mitochondrial outer membrane protein, FASEB J. 25 (2011) 4522–4530.

[54] P. Mentesana, J. Konopka, Mutational analysis of the role of N-glycosylation in alpha-factor receptor function, Biochemistry 40 (2001) 9685–9694.

[55] A. Brown, S. Dyos, M. Whiteway, J. White, M. Watson, M. Marzioch, J. Clare, D. Cousens, C. Paddon, C. Plumpton, M. Romanos, S. Dowell, Functional coupling of mammalian receptors to the yeast mating pathway using novel yeast/mammalian G protein alpha-subunit chimeras, Yeast 16 (2000) 11–22.
[56] S.R. George, B.F. O'Dowd,, S.P. Lee, G-protein-coupled receptor oligomerization and its potential for drug discovery, Nat. Rev. Drug Discov. (2002) 808–820.
[57] M.J. Lohse, Dimerization in GPCR mobility and signaling, Curr. Opin. Pharmacol. 10 (2010) 53–58.
[58] G. Milligan, G protein-coupled receptor dimerization: function and ligand pharmacology, Mol. Pharmacol. 66 (2004) 1–7.
[59] S.C. Prinster, C., H., R.A. Hall, Heterodimerization of G protein-coupled receptors: specificity and functional significance, Pharmacol. Rev. 57 (2005) 289–298.
[60] S. Terrillon, T. Durroux, B. Mouillac, A. Breit, M.A. Ayoub, M. Taulan, R. Jockers, C. Barberis, M. Bouvier, Oxytocin and vasopressin V1a and V2 receptors form constitutive homo- and heterodimers during biosynthesis, Mol. Endocrinol. 17 (2003) 677–691.
[61] S. Angers, A. Salahpour, M. Bouvier, Dimerization: an emerging concept for G protein-coupled receptor ontogeny and function, Annu. Rev. Pharmacol. Toxicol. 42 (2002) 409–435.
[62] L.F. Agnati, K. Fuxe, M. Zoli, C. Rondanini, S.O. Ogren, New vistas on synaptic plasticity: the receptor mosaic hypothesis of the engram, Med. Biol. 60 (1982) 183–190.
[63] S.C. Prinster, C. Hague, R.A. Hall, Heterodimerization of G protein-coupled receptors: specificity and functional significance, Pharmacol. Rev. 57 (2005) 289–298.
[64] G. Milligan, The prevalence, maintenance, and relevance of G protein-coupled receptor oligomerization, Mol. Pharmacol. 84 (2013) 158–169.
[65] F.H. Marshall, K.A. Jones, K. Kaupmann, B. Bettler, GABAB receptors — the first 7TM heterodimers, Trends Pharmacol. Sci. 20 (1999) 396–399.
[66] C. Lavoie, J.F. Mercier, A. Salahpour, D. Umapathy, A. Breit, L.R. Villeneuve, W.Z. Zhu, R.P. Xiao, E.G. Lakatta, M. Bouvier, T.E. Hebert, Beta 1/beta 2-adrenergic receptor heterodimerization regulates beta 2-adrenergic receptor internalization and ERK signaling efficacy, J. Biol. Chem. 277 (2002) 35402–35410.
[67] J.F. Mercier, A. Salahpour, S. Angers, A. Breit, M. Bouvier, Quantitative assessment of beta 1- and beta 2-adrenergic receptor homo- and heterodimerization by bioluminescence resonance energy transfer, J. Biol. Chem. 277 (2002) 44925–44931.
[68] C. Lavoie, T.E. Hebert, Pharmacological characterization of putative beta1–beta2-adrenergic receptor heterodimers, Can. J. Physiol. Pharmacol. 81 (2003) 186–195.
[69] C. Romano, W.L. Yang, K.L. O'Malley, Metabotropic glutamate receptor 5 is a disulfide-linked dimer, J. Biol. Chem. 271 (1996) 28612–28616.
[70] B. Wu, E.Y. Chien, C.D. Mol, G. Fenalti, W. Liu, V. Katritch, R. Abagyan, A. Brooun, P. Wells, F.C. Bi, D.J. Hamel, P. Kuhn, T.M. Handel, V. Cherezov, R.C. Stevens, Structures of the CXCR4 chemokine GPCR with small-molecule and cyclic peptide antagonists, Science 330 (2010) 1066–1071.
[71] T.E. Hebert, S. Moffett, J.P. Morello, T.P. Loisel, D.G. Bichet, C. Barret, M. Bouvier, A peptide derived from a beta2-adrenergic receptor transmembrane domain inhibits both receptor dimerization and activation, J. Biol. Chem. 271 (1996) 16384–16392.
[72] C. Shi, S. Kaminskyj, S. Caldwell, M.C. Loewen, A role for a complex between activated G protein-coupled receptors in yeast cellular mating, Proc. Natl. Acad. Sci. U. S. A. 104 (2007) 5395–5400.
[73] M. Dosil, J.B. Konopka, Strategies for isolating constitutively active and dominant-negative pheromone receptor mutants in yeast, Methods Enzymol. 485 (2010) 329–348.
[74] C. Xue, Y.P. Hsueh, J. Heitman, Magnificent seven: roles of G protein-coupled receptors in extracellular sensing in fungi, FEMS Microbiol. Rev. 32 (2008) 1010–1032.
[75] P.C. Ng, J.G. Henikoff, S. Henikoff, PHAT: a transmembrane-specific substitution matrix predicted hydrophobic and transmembrane, Bioinformatics 16 (2000) 760–766.
[76] M. Clamp, J. Cuff, S.M. Searle, G.J. Barton, The Jalview Java alignment editor, Bioinformatics 20 (2004) 426–427.